Evaluation of a diverse population of morphed human body models for prediction of vehicle occupant crash kinematics

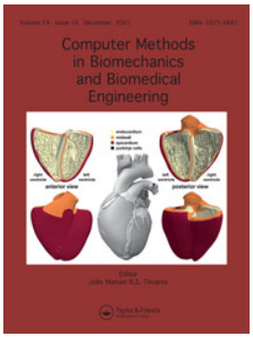

Taylor & Francis
Taylor & Francis Group

Computer Methods in Biomechanics and Biomedical Engineering

ISSN: (Print) (Online) Journal homepage: https://www.tandfonline.com/loi/gcmb20

Evaluation of a diverse population of morphed human body models for prediction of vehicle occupant crash kinematics

Karl-Johan Larsson, Bengt Pipkorn, Johan Iraeus, Jason Forman & Jingwen Hu

To cite this article: Karl-Johan Larsson, Bengt Pipkorn, Johan Iraeus, Jason Forman & Jingwen Hu (2021): Evaluation of a diverse population of morphed human body models for prediction of vehicle occupant crash kinematics, Computer Methods in Biomechanics and Biomedical Engineering, DOI: 10.1080/10255842.2021.2003790

To link to this article: https://doi.org/10.1080/10255842.2021.2003790

Published online: 29 Nov 2021.

COMPUTER METHODS IN BIOMECHANICS AND BIOMEDICAL ENGINEERING
https://doi.org/10.1080/10255842.2021.2003790

Evaluation of a diverse population of morphed human body models for prediction of vehicle occupant crash kinematics

Karl-Johan Larsson[a,b], Bengt Pipkorn[a,b], Johan Iraeus[a], Jason Forman[c] and Jingwen Hu[d]

[a]Department of Mechanics and Maritime Sciences, Division of Vehicle Safety, Chalmers University of Technology, Gothenburg, Sweden; [b]Autoliv Research, Vårgårda, Sweden; [c]Center for Applied Biomechanics, University of Virginia, Charlottesville, VA, USA; [d]Department of Mechanical Engineering, University of Michigan Transportation Research Institute, Ann Arbor, MI, USA

ABSTRACT

Morphing can be used to alter human body models (HBMs) to represent a diverse population of occupants in car crashes. The mid-sized male SAFER HBM v9 was parametrically morphed to match 22 Post Mortem Human Subjects, loaded in different configurations. Kinetics and kinematics were compared for the morphed and baseline HBMs. In frontal impacts, the morphed HBMs correlated closer with the kinematics of obese subjects, but lower to small females. In lateral impacts HBM responses were too stiff. This study outlines a necessary evaluation of all HBMs that should be morphed to represent the diverse population in vehicle safety evaluations.

ARTICLE HISTORY
Received 6 November 2020
Accepted 4 November 2021

KEYWORDS
Diversity; females; human body model; morphing; obesity; safety

Introduction

Elderly, obese and female occupants are vulnerable sub-populations at increased risk of sustaining injury in vehicle crashes (Viano et al. 2008; Jehle et al. 2012; Ridella et al. 2012; Carter et al. 2014; Forman et al. 2019). Overall, the accident injury risk has decreased in accidents involving newer vehicles (post model year 2009), however the vulnerable sub-populations remain at increased risk (Forman et al. 2019). Thus, injury risk assessment tools that can be used to develop vehicles and safety systems providing enhanced safety performance for all occupants are required.

Traditionally, occupant injury risk assessment has been carried out using anthropomorphic test devices (ATDs) in crash tests. ATDs representing the adult occupant population are available in three sizes, a 50th percentile male, a 95th percentile male, and a 5th percentile female. These sizes are based on U.S. population measurements of height and weight from the 1970s (Schneider et al. 1983). If compared to more recent U.S. population measurements, the 50th and 95th male ATD weights correspond to the 33rd and 81st percentile of body mass (Reed and Rupp 2013).

Finite element (FE) human body models (HBMs) are human occupant surrogates that can be used as an alternative, or a complement, to ATDs in mathematical simulations of crash scenarios. HBMs, in contrast to current ATDs, include detailed representations of the human anatomy and allow for calculating deformations and resulting stresses and strains throughout the internal body parts. Hence, physical variables mechanically related to injury, such as rib strain (Trosseille et al. 2008), can be evaluated using HBMs and related to rib fracture risk (Forman et al. 2012).

Examples of HBMs include; the Total Human Model for Safety (THUMS) (Shigeta et al. 2009), the Global Human Body Model Consortium (GHBMC) (Gayzik et al. 2012) and the SAFER (Iraeus and Pipkorn 2019) HBMs. The GHBMC and THUMS HBMs are available in the same adult occupant sizes as the ATDs while the SAFER HBM only represents the 50th percentile male occupant anthropometry. Current HBMs, while suitable for studying the interaction of human anatomy in conjunction with the vehicle and safety system, are not equipped to study what effect sex, age, stature and weight variations have on the interaction between human anatomy, vehicles and safety systems, beyond the traditionally considered ATD sizes.

In contrast to physical ATDs, the geometry of the HBMs can be modified to enable representation of other anthropometries. Using parametric morphing is one way of creating a wider range of model anthropometrics. The development of a parametric HBM

CONTACT Karl-Johan Larsson karl-johan.larsson@autoliv.com

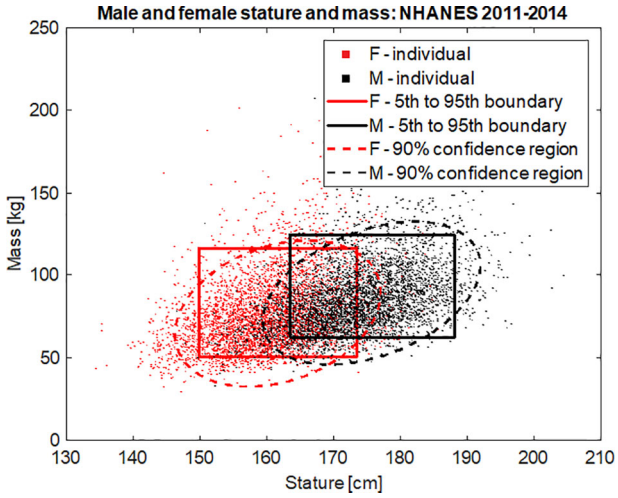

Figure 1. Stature and mass of males and females from NHANES 2011-2014 data. Univariate 5^{th}-95^{th} percentile bounds (boxes) and bivariate 90% probability regions (ellipses).

morphing method (Hwang et al. 2016), utilizing statistical human shape-based geometry models, has enabled rapid development of HBMs geometrically representing a wide range of statures, weights and ages for adult male and female occupants. Using this method, the geometry of an existing HBM is morphed to fit target geometries generated by statistical shape modeling of the ribcage, pelvis, femora, tibiae and the body surface (Reed and Ebert 2013; Klein et al. 2015; 2015; Wang et al. 2016). By using the statistical geometry models, the resulting HBM geometry will represent an average individual within the sub-population, provided by the morphing parameters, sex, age, stature and body mass index (BMI).

Parametric HBM morphing has enabled simulation studies exploring the effect of anthropometric variables on occupant injury risk (Hu et al. 2019). Before such studies can guide the design of safety systems, it is important that the morphed HBMs are validated to ensure a high level of biofidelity. Previous validation efforts of parametrically morphed HBMs have reconstructed individual Post Mortem Human Subject (PMHS) tests to compare results between morphed HBMs to specific PMHSs. Predictions of obese versions of the THUMS v4 (Zhang et al. 2017) and the GHBMC M50-O (Gepner et al. 2018) HBMs, created using parametric morphing, have been compared to corresponding PMHS results in frontal impacts. The morphed THUMS v4 was reported to account for the effects of obesity on excursion kinematics and prediction of injury risk indicators, such as acceleration and chest deflection. The morphed GHBMC failed to predict the PMHS submarining (pelvis sliding under the lap belt). In another study, Hwang et al. (Hwang et al. 2020) evaluated the THUMS v4 model as parametrically morphed to match the sex, age, stature and BMI of seven male PMHSs. The morphed THUMS v4 models predicted lateral impact force histories closer to each PMHS test result compared to the baseline, i.e. not morphed, HBM. Morphing of the SAFER HBM v9 to elderly female PMHSs evaluated in side impact increased kinematic correlation between model and test subjects, but reduced correlation for chest deflections (Larsson et al. 2019).

Thus, previous research indicates that the predictive capabilities of parametrically morphed HBMs depend on which version of HBM that is morphed, the impact configuration, and the subject anthropometry of the PMHS in the test reconstruction. Therefore, it is important to investigate the predictive capability of HBMs morphed to match a wide range of anthropometries in several impact configurations, before these models are used to develop safety systems for the diverse population.

The aim of this study was to evaluate the capability of parametrically morphed HBMs to predict PMHS kinematics of both sexes, for a variety of body compositions, in a number of different loading directions and severities. An additional aim involved evaluating for which anthropometries and load cases the morphed models provide predictive benefits over the baseline 50^{th} percentile male model.

Materials and methods

In this study the SAFER HBM v9 was parametrically morphed to match the sex, age, stature and BMI of 19 PMHSs tested in 22 different impacts (eight test configurations). The impact directions varied from near-side lateral to far-side oblique. Each PMHS test was modeled and replicated with both morphed and baseline HBMs in the FE solver LS-DYNA (LS-Dyna, R9.2.0 R119543, LSTC). For objective evaluation of model to test correlation, the model predictions of kinematics and kinetics were compared to corresponding individual PMHS test results by means of magnitude weighted CORA cross-correlation rating (Gehre et al. 2009).

Selection of PMHS tests for HBM evaluation

The population of interest was defined based on male and female stature and weight variation, according to the U.S 2011-2014 national health and nutrition examination survey (NHANES) (Fryar et al. 2016). This population roughly matches the population of

vehicle occupants, i.e. the population the morphed HBMs will represent. To define stature and weight ranges, 90% probability regions of a bivariate normal distribution were calculated according to (Brolin et al. 2012), also considering the NHANES weighting factors. Figure 1 shows the male and female individual NHANES samples, and the 90% male and female ranges. The univariate 5th to 95th percentile regions are also shown for comparison. To maximize the validity of the morphed HBMs, the PMHS tests used for HBM evaluation should ideally be evenly distributed within these elliptical regions.

Additional PMHS test inclusion criteria include:

- PMHS tests reproducing typical vehicle accident scenarios (any direction from far-side to near-side lateral) using whole-body PMHSs.
- Documentation of un-scaled test results from each individual PMHS
- Only adult PMHSs (aged from 18 years old)

HBM morphing to selected PMHSs

The parametric HBM morphing method utilizing statistical human shape target geometries previously presented in (Hwang et al. 2016) was used for morphing the SAFER HBM v9 to match each of the 19 PMHSs, based on each subject's sex, age, stature and BMI as morphing parameters, resulting in 19 morphed HBMs. The baseline SAFER HBM will be referred to as B-HBM and the morphed versions as M-HBMs. Following the morphing step, the density of flesh material in the M-HBMs' arms, legs and trunk, were uniformly scaled to achieve the target PMHS mass. Subsequently, the M-HBMs were inspected for defects with the potential of degrading the numerical performance of the model, i.e. contact surface intersections or degraded element quality compared to the B-HBM. Any defects were eliminated by small nodal movements.

HBM reconstructions of PMHS tests

Each PMHS test was reconstructed using both the B-HBM and the M-HBM corresponding to each specific PMHS in the test. All FE models representing the boundary conditions, i.e. each physical test environment, have previously been described in the literature, see Table A1, Appendix A. Contact between HBM and test environment as well as contact between HBM and seat belt was modelled using segment-based penalty contacts in LS-Dyna (*AUTOMATIC_SURFACE_TO_SURFACE, SOFT = 2, SBOPT = 3, DEPTH = 5, VDC = 20) with a friction coefficient of 0.3 (Kang et al. 2018).

All tests were reconstructed based on descriptions in the PMHS test reports. The seatbelt routing was modeled based on pre-test photography, measurements and digitized coordinates of markers on the belt centerline (not available for all tests). Hereafter, this belt path is referred to as the nominal shoulder belt path. However, since neither the B-HBM, nor the M-HBM, corresponded exactly to the actual PMHS body shape, the shoulder belt path (the segment of the seatbelt from the D-ring or retractor to the belt buckle) was expected to deviate from the actual shoulder belt wrapping in the physical test. Further, it was hypothesized that the torso shape-driven differences in shoulder belt routing could influence the HBM predictions. Therefore, in an additional analysis, three additional shoulder belt paths (High, Mid and Low) were modeled for any load cases in which the shoulder belt was expected to limit the PMHS excursion, including the frontal oblique near-side, frontal and the far-side tests (all referred to as frontal impacts hereafter). The High routing was guided across the sternum at the level of the 1st ribs, while the Mid and Low routings crossed at the 3rd and 6th rib level, respectively (Figure 2). The locations of seatbelt anchorage points were not modified. Seatbelt system functions such as pre-tensioning and load limiting were modelled according to the specifications extracted from each test publication (Table 1).

As HBM kinematic predictions have been shown to be sensitive to initial posture (Piqueras-Lorente et al. 2018), the M-HBMs initial postures were carefully adjusted to match target coordinates describing each PMHS's initial posture. The coordinates were based on available PMHS test documentation regarding initial position, including photographs, measurements and digitized coordinates of bony landmarks. To ensure comparability of the initial postures of the B-HBM and the PMHS (Figure 3), whose stature and BMI differed in most cases, the target coordinates for initial posture in each test reconstruction were obtained by scaling the M-HBM posture target coordinates according to the stature ratio between the B-HBM and the PMHS. All HBMs were positioned in the FE test environment using LS-Dyna pre-simulations.

The correlation between HBM predictions and PMHS results were quantified using the CORA cross-correlation method (Gehre et al. 2009) with recommended parameters according to (Thunert 2017)

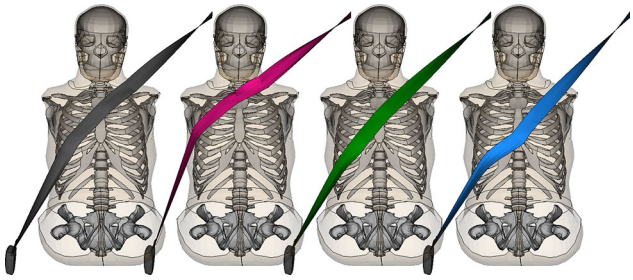

Figure 2. Shoulder belt routings varied over HBM sternum. Left to right is Nominal, High, Mid and Low. M-HBM in simulation of Test s0135, Series 5.

(CORAplus v4.0.4, PDB). The CORA score spans between 0 to 1 (higher is better) rating the correlation between the simulation predictions and physical test result signals, based on phase, size and shape similarity. This method has previously been used to rate HBM prediction to individual PMHS result correlation (Hwang et al. 2016; Larsson et al. 2019; Hwang et al. 2020). Kinetic quantities evaluated include seatbelt or impactor forces, while kinematic quantities evaluated include occupant excursion in frontal impacts, spine lateral velocity (integrated from accelerometers) and chest deflections (individually normalized by initial chest dimension) in lateral impacts. A more comprehensive description of evaluated signals can be found in Appendix A. For each test reconstruction a resulting CORA rating within each quantity (force or motion) was calculated by weighting the different sub-components. Weights were calculated based on the peak magnitude of each test signal.

As a guideline to classify goodness of fit between the HBM and PMHS based on resulting CORA rating, an adapted version of the ISO/TR 9790:1999 biofidelity scale was used; unacceptable $< 0.26 \leq$ marginal $< 0.44 \leq$ fair $< 0.65 \leq$ good $< 0\ .86 \leq$ excellent.

Furthermore, all results and the CORA ratings were visually inspected for trends, such as increasing or decreasing excursions or correlations, with respect to the morphing parameters and impact speed. Also, the animations of the simulation results were visually inspected for non-linear events, such as the presence of submarining or the HBM sliding out of the shoulder belt, i.e. the shoulder belt webbing sliding laterally past the acromion.

Results

Selection of PMHS tests for HBM evaluation and morphing to selected PMHSs

In total, 22 published PMHS tests performed with 19 different subjects in eight test setups met the inclusion criteria (Table 1). Impact directions included near-side lateral, frontal oblique 30° near-side, frontal and frontal oblique 60° far-side. Eight test subjects (seven PMHSs) were female and 12 subjects (in 14 tests) were male (Table 2). Age, stature, and BMI of the seven females ranged (mean ± std. dev.) between 51-83 years (64.9 ± 12.2), 152-167 cm (160.6 ± 5.9) and 14-40 kg/m^2 (22.7 ± 9.1). For the 12 males, age, stature and BMI ranged between 34-87 years (61.7 ± 16.1), 160-189 cm (176.6 ± 8.4) and 18-35 kg/m^2 (24.8 ± 4.8).

Examples of created M-HBMs and the B-HBM are displayed in Figure 4.

HBM reconstruction of PMHS tests

Frontal impacts

The resulting CORA ratings for the frontal impacts with nominal shoulder belt routing, and the range of CORA ratings obtained when shoulder belt routing was varied are presented in Table 3. Appendix B Figures B1-B10 show examples of PMHS, M-HBM and B-HBM result time histories for each of the frontal impact setups. Example frames for visual comparison of PMHS test video and HBM simulation animations for each frontal impact setup are shown in Appendix C Figures C1-C5. For both the B-HBM and the M-HBMs, the kinetic CORA ratings (seatbelt forces), ranged from 0.55 to 0.92, corresponding to fair to excellent biofidelity. The kinematic CORA ratings ranged from 0.61 to 0.86, corresponding to fair to excellent biofidelity. The differences in CORA rating between the B-HBM and the M-HBMs were small in the majority of the tests. Exceptions included Tests 1263 and 1333, representing obese subjects, where the M-HBMs obtained higher CORA ratings, by predicting increased forward excursions compared to the B-HBM. However, obese M-HBMs still underpredicted the obese PMHS pelvis forward excursion (Figure 5). Further, in Tests 1262 and s0213 the B-HBM obtained a higher CORA rating compared to the M-HBMs. In Test 1262, the belt slipped off the shoulder of the M-HBM (for all initial shoulder belt positions), changing excursion in contrast to the PMHS and B-HBM. For Test s0213, Series 4, the small female M-HBM rebounded earlier than the small female PMHS and underpredicted the forwards excursions, while the taller B-HBM overpredicted, the forwards excursions. Similar results were predicted by the M-HBM in Test s0211, representing another small female PMHS in the same test series. The earlier rebound is shown for the head forward excursion

Table 1. PMHS tests modeled in the study. Series refers to a specific test configuration, and Impact Direction describes the principal direction of acceleration. Publication is a reference describing the test and test results. Test ID is the identification number of the test in the publication. Restraints encodes the restraint system(s) used in the test. ΔV is the test velocity.

Series	Impact Direction	Publication	Test ID	Restraint[1]	ΔV (km/h)
1	Oblique Near-Side 30°	(Lopez-Valdes et al. 2016)	1441	SB + LL + LPT	35
2	Frontal	(Michaelson et al. 2008)	1262	SB	49
			1263	SB	47
		(Forman et al. 2009)	1333	SB + PT + PLL	49
3	Frontal	(Lopez-Valdes et al. 2018)	1761	SB + LL, Airbag	35
4	Frontal	(Shaw et al. 2017)	s0211	SB + LL	30
			s0213	SB + LL	30
5	Oblique Far-Side 60°	(Forman et al. 2013)	s0124	SB + PT + LL	34
			s0135	SB + PT + LL	34
6	Lateral	(Miller et al. 2013)	NBA1004A	None	11
			NBA1005A	None	11
			NBA1006A	None	11
			NBA1006B	None	29
			NBA1007A	None	11
			NBA1108A	None	11
7	Lateral	(Wood et al. 2014)	NBA1109A	None	11
			NBA1110A	None	11
			NBA1110B	None	22
			NBA1213A	None	11
			NBA1213B	None	22
8	Lateral	(Shurtz et al. 2018)	1701	SB + LL + PT, Airbag	50[2]
			1702	SB + LL + PT, Airbag	50[2]

[1] SB = seatbelt, LL = retractor load limiter, PLL = progressive retractor load limiter, PT = retractor pre-tensioning, LPT = lap belt pre tensioning. 2 Sled test simulates door intrusion and lateral acceleration from a 50 km/h moving deformable barrier to vehicle impact test.

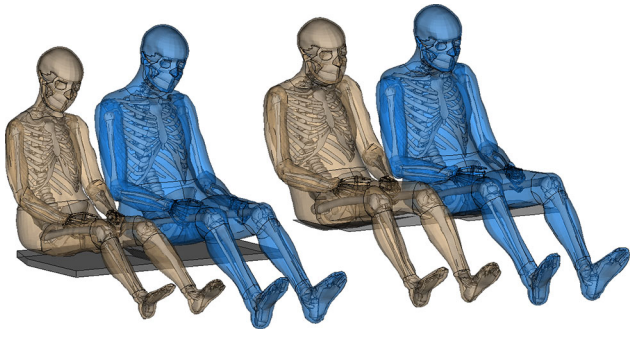

Figure 3. Examples of morphed and baseline HBMs (blue HBM) initial postures. To the left is morphed and baseline HBM from Test s0211, Series 4. To the right is Morphed and Baseline HBM from Test 1441, Series 1.

(Figure 6) in which the M-HBMs reached maximum excursion 15 ms (Test s0211) and 22 ms (Test s0213) earlier than the corresponding PMHSs.

Additionally, as shown in Table 3, the HBM to PMHS CORA ratings were only marginally affected by varying the initial shoulder belt position. The only exception was found in Series 5 in which all HBMs slipped out of the shoulder belt, bar the M-HBM in Test s0135 with High shoulder belt routing (Figure 2). This reduced lateral excursion and resulted in a 0.66 kinematic CORA rating for this M-HBM.

Across all frontal impacts, no trends, such as an increase or decrease, with respect to morphing parameters or impact speed for peak excursions or CORA ratings, were observed for the M-HBMs or B-HBM.

Table 2. PMHSs included in the modeled tests. Tests NBA1006B, NBA1110B and NBA1213B used the same PMHS as the test with same numbering ending with an 'A' but impacted the opposite side.

Series	Test ID	Sex (M/F)	Age (Years)	Stature (cm)	Mass (kg)	BMI (kg/m^2)
1	1441	M	60	171	65	22
2	1262	M	51	175	55	18
	1263	F	57	165	109	40
	1333	M	54	189	124	35
3	1761	M	74	167	66	24
4	s0211	F	57	162	40	15
	s0213	F	65	152	47	20
5	s0124	M	44	182	86	26
	s0135	M	61	178	79	25
6	NBA1004A	M	66	173	79	26
	NBA1005A	M	51	183	98	29
	NBA1006A	M	34	188	102	29
	NBA1006B	M	34	188	102	29
	NBA1007A	M	87	175	72	24
	NBA1108A	M	85	178	56	18
7	NBA1109A	F	51	157	68	28
	NBA1110A	F	80	167	39	14
	NBA1110B	F	80	167	39	14
	NBA1213A	M	73	160	53	21
	NBA1213B	M	73	160	53	21
8	1701	F	61	166	65	24
	1702	F	83	155	44	18

Lateral impacts

For the lateral impacts, the kinetic CORA scores ranged from 0.57 to 0.88, corresponding to fair to excellent biofidelity (Table 4). Appendix B Figures B11-B19 show examples of PMHS, M-HBM and B-HBM result time histories for each of the lateral impact setups. Example frames for visual comparison

of PMHS test video and HBM simulation animations for each lateral impact setup are shown in Appendix C Figures C6-C8. The kinematic CORA scores ranged from 0.63 to 0.89 for lateral velocity and 0.18 to 0.82 for chest deflections, corresponding to unacceptable to excellent biofidelity. The major difference between the B-HBM and the M-HBMs was seen for chest deflections, where the B-HBM showed results closer to the PMHSs for most of the cases.

No trends with respect to morphing parameters or impact speeds were seen. However, a general observation of overestimated impactor force and underestimated chest deformation was made for lateral impacts, for both the B-HBM and the M-HBMs, i.e. the HBMs were too stiff. Typical force-deflection responses for the B-HBM, M-HBMs and the PMHSs are represented by Test NBA1004A (Figure 7).

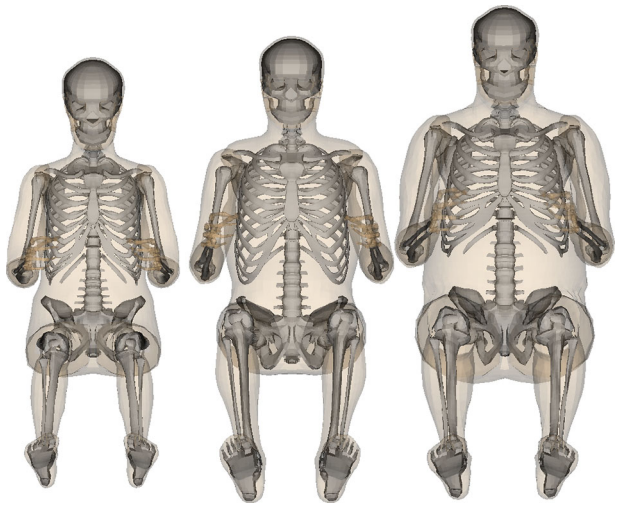

Figure 4. Morphed and baseline HBMs. Left: M-HBM in Test s0211, Series 4, Middle: B-HBM, Right: M-HBM in Test 1333, Series 2.

Discussion

The wide range of subject statures and masses as well as the wide range of crash scenarios makes the current study one of the most comprehensive for the evaluation of morphed HBMs. Comparing HBM predictions to several different subjects in different impact conditions made identifying HBM predictions, deviating from several individual PMHS results, possible across test configurations, i.e. HBM stiffness, discussed below. Hence, the results are robust, reducing the risk of being influenced by individual subjects and test conditions. However, including several test series,

Table 3. Simulation CORA Ratings for Series 1-5, Morphed and Baseline HBMs correlation to PMHS kinematics and Seatbelt forces. According to Nominal shoulder belt routing (range High/Mid/Low shoulder belt).

		Excursion Kinematics		Seatbelt Forces	
Series	Test ID	Morphed HBM	Baseline HBM	Morphed HBM	Baseline HBM
1	1441	0.83(0.81-0.84)	0.79(0.79-0.80)	0.87(0.87-0.88)	0.86(0.86-0.87)
2	1262	0.68(0.67-0.74)	0.82(0.80-0.83)	0.70(0.70-0.77)	0.68(0.67-0.68)
	1263	0.72(0.72-0.74)	0.61(0.61-0.63)	0.55(0.55-0.58)	0.57(0.58-0.58)
	1333	0.75(0.74-0.76)	0.66(0.66-0.67)	0.76(0.76-0.77)	0.59(0.59-0.61)
3	1761	0.77(0.77-0.78)	0.76(0.76-0.77)	0.84(0.84-0.84)	0.85(0.85-0.85)
4	s0211	0.66(0.67-0.67)	0.64(0.66-0.69)	0.88(0.86-0.88)	0.92(0.88-0.92)
	s0213	0.67(0.66-0.67)	0.76(0.73-0.77)	0.81(0.79-0.81)	0.79(0.79-0.83)
5	s0124	0.81(0.79-0.81)	0.85(0.84-0.85)	0.82(0.82-0.86)	0.82(0.82-0.83)
	s0135	0.78(0.66-0.86)	0.83(0.78-0.85)	0.89(0.87-0.90)	0.75(0.74-0.76)

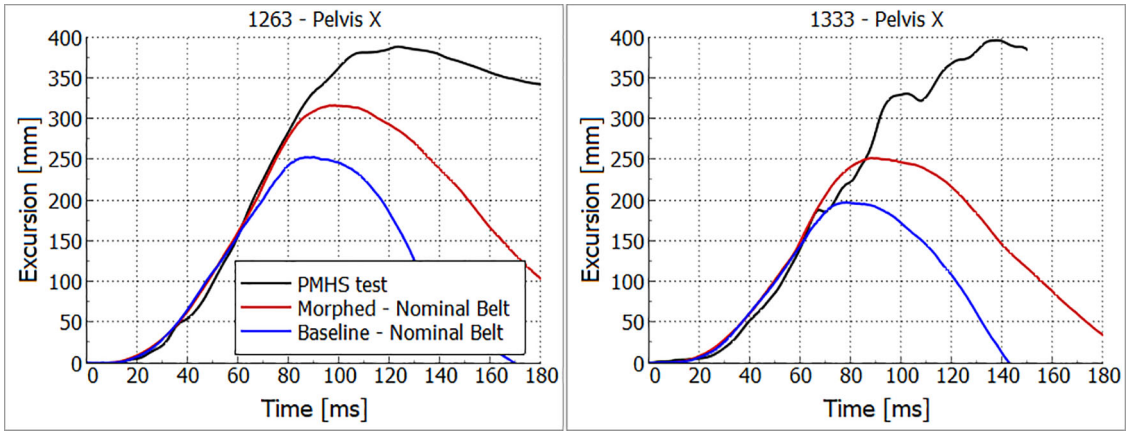

Figure 5. Pelvis forwards (X) excursions from Series 2, Tests 1263 (left) and 1333 (right). PMHS test results (black), Morphed (red) and Baseline (blue) HBMs with nominal shoulder belt path.

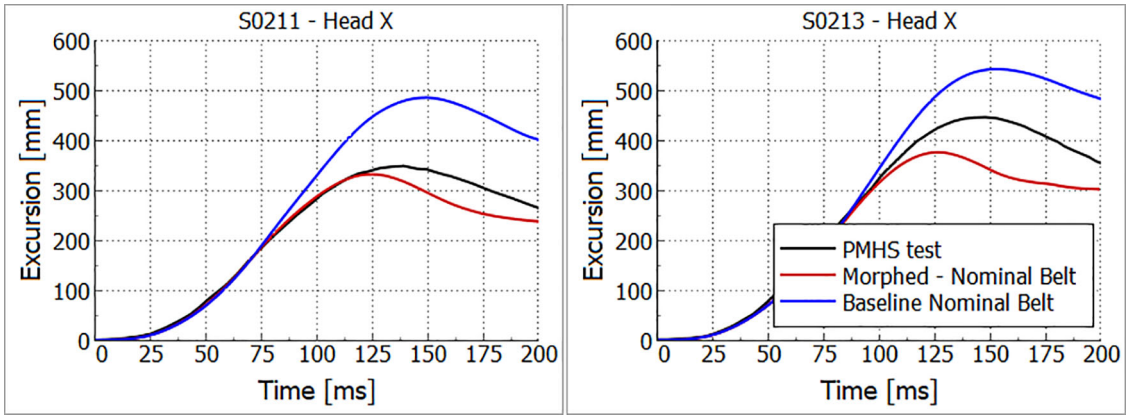

Figure 6. Head forwards (X) excursions from Series 4, Tests s0211 and s0213. PMHS test results (black), Morphed (red) and Baseline (blue) HBMs with nominal shoulder belt path.

Table 4. Simulation CORA ratings for Lateral impacts, Series 6, 7 and 8. Morphed and Baseline HBMs correlation to PMHS kinematics, chestband deflections and impactor forces.

		Lateral Velocity Kinematics		Deflections		Impactor Forces	
Series	Test ID	Morphed HBM	Baseline HBM	Morphed HBM	Baseline HBM	Morphed HBM	Baseline HBM
6	NBA1004A	0.65	0.68	0.61	0.64	0.70	0.80
	NBA1005A	0.72	0.68	0.63	0.59	0.82	0.85
	NBA1006A	0.65	0.63	0.56	0.51	0.84	0.82
	NBA1006B	0.70	0.75	0.55	0.47	0.81	0.86
	NBA1007A	0.72	0.75	0.47	0.59	0.76	0.83
	NBA1108A	0.76	0.78	0.65	0.83	0.74	0.85
7	NBA1109A	0.75	0.82	0.36	0.37	0.61	0.67
	NBA1110A	0.76	0.77	0.42	0.76	0.62	0.65
	NBA1110B	0.74	0.77	0.38	0.78	0.59	0.60
	NBA1213A	0.73	0.74	0.73	0.82	0.67	0.57
	NBA1213B	0.89	0.88	0.61	0.81	0.77	0.73
						Seatbelt forces	
8	1701	0.88	0.86	0.18	0.43	0.85	0.88
	1702	0.83	0.80	0.33	0.68	0.73	0.61

each originally performed for a certain purpose, resulted in a mix of restraint conditions, impact speeds and different results measured across the used reference data. Each PMHS result was a product of both the individual PMHS characteristics as well as the specific test setup. This may partly explain why it was not possible to observe a trend in HBM predictions with respect to the morphing parameters and impact speeds for this reference data. Including reference data from more test subjects in each test series, where available, could potentially reveal trends, at least within each test configuration.

In Figure 8, the mass and stature of each included PMHS were compared to the 90% male and female population probability regions. Generally, the PMHSs span the stature-mass space. However, except for the obese male and female subjects (Tests 1263, 1333), high BMI reference PMHS tests are lacking as no suitable tests were found. Additional male and female subjects of higher BMI tested in oblique impact directions will increase the representation of the diverse population in the reference data.

In most of the cases both the B-HBM and M-HBMs obtained CORA ratings corresponding to good biofidelity according to the adapted biofidelity ranking scale. This indicates that both models, the B-HBM and the M-HBMs, are useful for evaluating occupant kinematics and boundary condition forces over a large range of occupant sizes. Still, some important exceptions emerged. For the obese subjects in Series 2, Tests 1263 (BMI 40 kg/m^2) and 1333 (BMI 35 kg/m^2), the M-HBMs correlated closer with the obese PMHSs, as they predicted greater forward excursions, most likely an effect of the increased mass in the M-HBM models. However, both the obese M-HBMs still underpredicted the large pelvis forward excursions observed in these tests (Figure 5), in which the lap belt penetrated deeply into the adipose tissue of the abdomen of both subjects who consequently submarined. The obese M-HBMs did not show as much adipose tissue compression and did not indicate any risk of submarining (example from Test 1333 in Appendix C Figure C2). These results correlate with previous conclusions based on a different HBM by Gepner

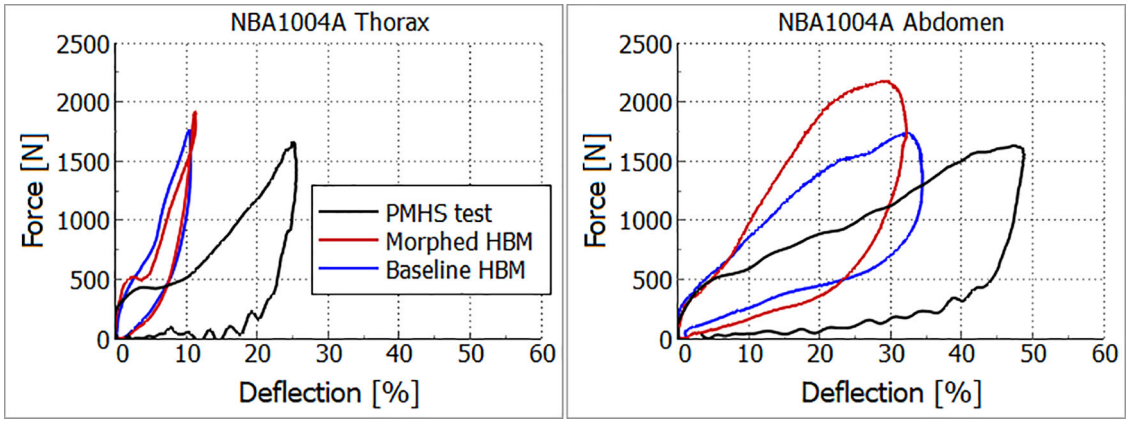

Figure 7. Force-deflection response for thorax and abdomen in Series 6, Test NBA1004A for PMHS test (black), Morphed (red) and Baseline (blue) HBMs.

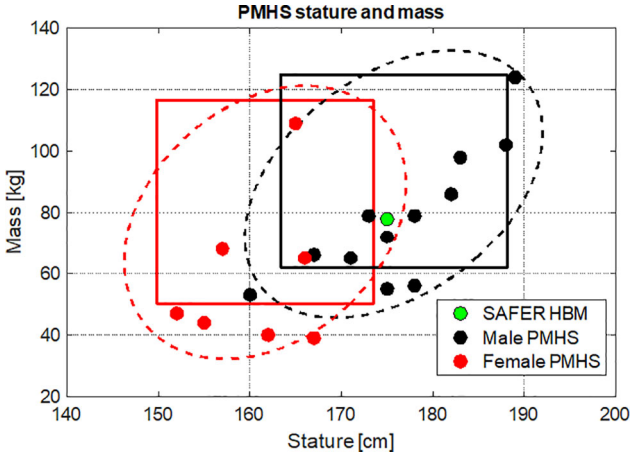

Figure 8. Stature and weight (body mass) of reference PMHS in this study. Dashed ellipses are 90% probability regions.

et al. (Gepner et al. 2018) who used an obese GHBMC model to reconstruct Test 1333 also used in this study. It was hypothesized that the GHBMC adipose soft tissue material model was too stiff to accurately model the lap belt interaction for obese subjects with a large amount of abdominal adipose tissue. This is most likely also true for the SAFER HBM v9 adipose soft tissue modeling. For the two small female subjects modeled in Series 4, Test s0211 (BMI 15 kg/m^2) and Test s0213 (BMI 20 kg/m^2), the M-HBMs rebounded 15 ms and 22 ms earlier than the PMHSs (Figure 6). Since the subject mass, sled acceleration and seatbelt force limiting levels matched in the M-HBM simulations and PMHS test, the earlier rebound is also an indication of a stiffer response. In the lateral impact tests in Series 6 and 7, where impact forces as well as chest deflections were available from the PMHS tests, both the M-HBMs and B-HBM exhibited a stiffer force-deflection response than the PMHSs (Figure 7). For Series 8, where unacceptable and marginal biofidelity was obtained for chest deflections, the corresponding PMHS normalized deflection magnitudes were consistently underestimated by the M-HBMs. Collectively, these results obtained from modeling different test subjects in different impact conditions, indicate that the M-HBMs are stiffer than the corresponding PMHSs. This issue needs to be addressed in future work.

The biofidelity rating scale applied for this study was based on the ISO/TR 9790:1999 biofidelity scale, intended for rating of side impact biofidelity in relation to reference corridors for specified reference tests. Therefore, the adapted scale applied here does not correspond to the ISO biofidelity ratings, but instead serves as CORA rating-based estimate of unacceptable to excellent HBM to individual PMHS correlation levels. Future work must further investigate the correlation evaluation and biofidelity criteria defined here.

Despite limitations of the current SAFER HBM v9, the M-HBMs derivatives can add value as occupant substitutes, as it was shown that the biofidelity was at least fair. A vehicle interior provides limited space for the safety systems to absorb the kinetic energy of occupants, and thus, added value is achieved by representing alternative occupant statures and weights to evaluate the effectiveness of different protective strategies for the diverse population.

In the current parametric morphing method implementation, the B-HBM geometry and mass have been adjusted, such that the M-HBM geometry represents an average individual of the same sex, age, stature and BMI as the corresponding PMHS. The use of averaged geometries does not produce a M-HBM geometry that fully matches the corresponding PMHS, as there are individual variations not described by the parametrized

geometry models. For example, under the current parameterization, the ribcage geometry model used can only represent 51%, and the pelvis geometry model 15% (Males) and 18% (Females), of the individual variation in their respective underlying datasets (Klein et al. 2015; Wang et al. 2016). By introducing more input parameters, e.g. seated height and chest circumference, to the parametric morphing method, the geometry of the morphed HBMs will be even closer to the actual PMHS. Some studies have taken this yet another step by creating individualized morphed HBMs, that matches PMHS skeletal geometry extracted from CT-scans, and external body surface measurements. However, so far these individualized HBMs have not provided any clear improvement over the parametric M-HBMs for the prediction of impact forces (Hwang et al. 2016), or kinematics and chest deflections (Larsson et al. 2019).

This study outlines a necessary evaluation for all HBMs that should be parametrically morphed to represent the diverse population of occupants and used in the development of future vehicles that are safe for all.

Conclusions

The kinematic response predictions of parametrically morphed and baseline SAFER HBMs were compared to individual PMHS test results representing a diverse occupant population in several impact directions.

- Resulting kinematic CORA cross-correlation ratings of HBMs ranged from 0.61-0.89 corresponding to fair to excellent biofidelity.
- Parametrically morphed HBMs obtained higher correlation ratings for obese PMHS frontal impact kinematics by predicting increased forward excursions.
- Parametrically morphed HBMs underpredicted small female PMHS forward excursion in frontal impacts.
- In lateral impacts, baseline HBMs predicted chest deflection magnitudes closer to the PMHSs.
- A general trend of too high stiffness in the HBM impact responses was identified and addressing this stiffness may provide additional benefits in morphed HBM predictive capabilities.
- The results from this study highlights the need of evaluating the predictive capabilities of an HBM morphed to a wide range of body sizes in several impact directions, before using the morphed HBMs as occupant substitutes for development of robust occupant protection systems.

Acknowledgements

The work was carried out at SAFER – Vehicle and Traffic Safety Centre at Chalmers, Sweden. The authors would like to thank several individuals who contributed with test data and test-setup models: Carl S. Miller at University of Michigan Transportation Research Institute; Greg Shaw, Bronislaw Gepner and Hamed Joodaki at University of Virginia Center for Applied Biomechanics; Ana Piqueras-Lorente at University of Zaragoza Impact Laboratory; Craig Markusic at Honda Research Americas and Krystoffer Mroz at Autoliv Research.

Disclosure statement

The authors declare no conflicts of interest.

Funding

The work performed in this study was funded by FFI-Strategic Vehicle Research and Innovation, by Vinnova, the Swedish Energy Agency and the Swedish vehicle industry.

ORCID

Karl-Johan Larsson http://orcid.org/0000-0001-9106-1252
Bengt Pipkorn http://orcid.org/0000-0002-9240-4517
Johan Iraeus http://orcid.org/0000-0001-9360-0707
Jason Forman http://orcid.org/0000-0001-8705-3997
Jingwen Hu http://orcid.org/0000-0001-6477-0360

References

Brolin E, Högberg D, Hanson L. 2012. Description of boundary case methodology for anthropometric diversity consideration. IJHFMS. 3(2):204–223.

Carter PM, Flannagan CAC, Reed MP, Cunningham RM, Rupp JD. 2014. Comparing the effects of age, BMI and gender on severe injury (AIS 3+) in motor-vehicle crashes. Accid Anal Prev. 72:146–160.

Eggers A, Wisch M, Ott J, Hynd D, Mühlbauer J, Fuchs T, Peldschus S, Pipkorn B, Mroz K. 2018. SENIORS Deliverable 2.5a - Updated Injury Criteria for the THOR. European Commission Eight Framework Programme Horizon 2020 GA No. 636136.

Forman JL, Kent RW, Mroz K, Pipkorn B, Bostrom O, Segui-Gomez M. 2012. Predicting rib fracture risk with whole-body finite element models: development and preliminary evaluation of a probabilistic analytical framework. In: 56th AAAM Annual Conference. Annals of Advances in Automotive Medicine. Vol. 56. p. 109–124.

Forman J, Lopez-Valdes FJ, Lessley D, Kindig M, Kent R, Bostrom O. 2009. The effect of obesity on the restraint of automobile occupants. In: 53rd AAAM Annual Conference. Annals of Advances in Automotive Medicine. Vol. 53. p. 25–40.

Forman J, Lopez-Valdes F, Lessley DJ, Riley P, Sochor M, Heltzel S, Ash J, Perz R, Kent RW, Seacrist T, et al.

2013. Occupant kinematics and shoulder belt retention in far-side lateral and oblique collisions: a parametric study. Stapp Car Crash J. 57(November):343–385.
Forman J, Poplin GS, Shaw CG, McMurry TL, Schmidt K, Ash J, Sunnevang C. 2019. Automobile injury trends in the contemporary fleet: Belted occupants in frontal collisions. Traffic Inj Prev. 20(6):607–612.
Fryar CD, Gu Q, Ogden CL, Flegal KM. 2016. Anthropometric reference data for children and adults: United States, 2011-2014. National Center for Health Statistics. Vital Health Stat. 3(39):9–15.
Gayzik FS, Moreno DP, Vavalle NA, Rhyne AC, Stitzel JD. 2012. Development of a full human body finite element model for blunt injury prediction utilizing a multi-modality medical imaging protocol. In: 12th International LS-DYNA Users Conference. p. 1–14.
Gehre C, Gades H, Wernicke P. 2009. Objective Rating of Signals Using Test and Simulation Responses. Enhanced Safety Vehicle (ESV). Paper Numb:09–0407.
Gepner BD, Joodaki H, Sun Z, Jayathirtha M, Kim T, Forman JL, Kerrigan JR. 2018. Performance of the obese GHBMC models in the sled and belt pull test conditions. In: Proceedings of IRCOBI Conference 2018. Athens.
Hu J, Zhang K, Reed MP, Wang JT, Neal M, Lin CH. 2019. Frontal crash simulations using parametric human models representing a diverse population. Traffic Inj Prev. 20(sup1):S97–S105.
Hwang E, Hu J, Chen C, Klein KF, Miller CS, Reed MP, Rupp JD, Hallman JJ. 2016. Development, evaluation, and sensitivity analysis of parametric finite element whole-body human models in side impacts. Stapp Car Crash J. 60(November):473–508.
Hwang E, Hu J, Reed MP. 2020. Validating diverse human body models against side impact tests with post-mortem human subjects. J Biomech. 98:109444.
Hwang E, Hallman J, Klein K, Rupp J, Reed M, Hu J. 2016. Rapid development of diverse human body models for crash simulations through mesh morphing. SAE Technical Paper 2016-01-1491.
Iraeus J, Pipkorn B. 2019. Development and validation of a generic finite element ribcage to be used for strain-based fracture prediction. In: Proceedings of IRCOBI Conference. Florence. p. 193–210.
Jehle D, Gemme S, Jehle C. 2012. Influence of obesity on mortality of drivers in severe motor vehicle crashes. Am J Emergency Med. 30(1):191–195.
Kang S, Chen C, Guha S, Paladugu M, Ramasamy MS, Gade L, Zhu F. 2018. LS-DYNA belted occupant model. In: 15th International LS-DYNA Users Conference. Detroit.
Klein KF, Hu J, Reed MP, Hoff CN, Rupp JD. 2015. Development and validation of statistical models of femur geometry for use with parametric finite element models. Ann Biomed Eng. 43(10):2503–2514.
Klein KF. 2015. Use of parametric finite element models to investigate effects of occupant characteristics on lower-extremity injuries in frontal crashes [PhD thesis]. University of Michigan.
Larsson K, Pipkorn B, Iraeus J, Bolte JH, IV Agnew AM, Hu J, Reed MP, Sunnevång C. 2019. Evaluation of the benefits of parametric human body model morphing for prediction of injury to elderly occupants in side impact. In: Proceedings of IRCOBI Conference. Florence. p. 150–174.
Lopez-Valdes FJ, Juste-Lorente O, Maza-Frechin M, Pipkorn B, Sunnevang C, Lorente A, Aso-Vizan A, Davidsson J. 2016. Analysis of occupant kinematics and dynamics in nearside oblique impacts. Traffic Inj Prev. 17(sup1):86–92.
Lopez-Valdes FJ, Mroz K, Eggers A, Pipkorn B, Muehlbauer J, Schick S, Peldschus S. 2018. Chest injuries of elderly postmortem human surrogates (PMHSs) under seat belt and airbag loading in frontal sled impacts: Comparison to matching THOR tests. Traffic Inj Prev. 19(sup2):S55–S63.
Michaelson J, Forman J, Kent R, Kuppa S. 2008. Rear seat occupant safety: kinematics and injury of PMHS restrained by a standard 3-point belt in frontal crashes. Stapp Car Crash J. 52(November):295–325.
Miller CS, Madura NH, Schneider LW, Klinich KD, Reed MP, Rupp JD. 2013. PMHS impact response in 3 m/s and 8 m/s nearside impacts with abdomen offset. Stapp Car Crash J. 57(November):387–425.
Pipkorn B, Larsson K-J, Perez Rapela D, Markusic C, Whitcomb B, Ayyagari M, Sunnevång C. 2018. Occupant protection in far-side impacts. In: Proceedings of IRCOBI Conference 2018. Vol. 46. Athens. p. 125–127.
Piqueras-Lorente A, Iraeus J, Lorente AI, López-Valdés FJ, Juste-Lorente Ó, Maza-Frechín M, Pipkorn B. 2018. Kinematic assessment of subject personification of human body models (THUMS). In: Proceedings of IRCOBI Conference. Athens. p. 191–206.
Reed MP, Ebert SM. 2013. Elderly occupants: posture, body shape, and belt fit. Ann Arbor: University of Michigan Transportation Research Institute Report No.: UMTRI-2013-26.
Reed MP, Rupp JD. 2013. An anthropometric comparison of current ATDs with the U.S. adult population. Traffic Inj Prev. 14(7):703–705.
Ridella SA, Rupp JD, Poland K. 2012. Age-Related differences in AIS 3+ crash injury risk, types, causation and mechanisms. In: Proceedings of IRCOBI Conference. Dublin, Ireland. p. 43–60.
Schneider LW, Robbins DH, Pflüg MA, Snyder RG. 1983. Development of anthropometrically based design specifications for an advanced adult anthropomorphic dummy family. Report No.: UMTRI-83-53-1.
Shaw G, Lessley D, Ash J, Poplin J, McMurry T, Sochor M, Crandall J. 2017. Small female rib cage fracture in frontal sled tests. Traffic Inj Prev. 18(1):77–82.
Shigeta K, Kitagawa Y, Yasuki T. 2009. Development of next generation human FE-model capable of organ injury prediction. Paper No. 09-0111. Proceedings of the 21st Enhanced Safety Vehicle (ESV) Conference.:1–20.
Shurtz BK, Agnew AM, Kang Y, Bolte J. 2018. Application of scaled deflection injury criteria to two small, fragile females in side impact motor vehicle crashes. SAE Technical Paper 2018-01-0542.:1–8.
Thunert C. 2017. CORAplus Release 4.0.4 User ' s Manual.
Trosseille X, Baudrit P, Leport T, Vallancien G. 2008. Rib cage strain pattern as a function of chest loading configuration. Stapp Car Crash J. 52(November):205–231.

Viano DC, Parenteau CS, Edwards ML. 2008. Crash injury risks for obese occupants using a matched-pair analysis. Traffic Inj Prev. 9(1):59–64.

Wang Y, Cao L, Bai Z, Reed MP, Rupp JD, Hoff CN, Hu J. 2016. A parametric ribcage geometry model accounting for variations among the adult population. J Biomech. 49(13):2791–2798.

Wood LK, Miller CS, Madura NH, Reed MP, Schneider LW, Klinich KD, Rupp JD. 2014. Response and tolerance of female and/or elderly PMHS to lateral impact. Stapp Car Crash J. 58(November):423–463.

Zhang K, Cao L, Wang Y, Hwang E, Reed MP, Forman J, Hu J. 2017. Impact response comparison between parametric human models and postmortem human subjects with a wide range of obesity levels. Obesity (Silver Spring). 25(10):1786–1794.

Appendix A.

Test setup modeling and studied test data

In this appendix, further details about the modelled test setups and the test data used for HBM to PMHS correlation evaluation is provided.

In Table A1, a brief description of each test environment model is presented, along with a reference where the environment model was previously used to perform HBM simulations of the studied test setup.

Below follows a description of all data used for HBM to PMHS correlation evaluation.

For the test series using a seatbelt, simulation seatbelt forces were extracted as cross-sectional forces from the locations along the model seatbelt webbing corresponding to the measurement locations of seatbelt forces in the tests. From Series 6 and 7, the impactor segment to HBM contact forces was extracted. For Series 6 this included Thorax, Abdominal, Pelvis Iliac Wing, Pelvis Greater Trochanter and Femur impactor forces. For Series 7, in addition, Head, Shoulder and Arm impactor forces were measured.

For the frontal, near-side and far-side oblique load cases (Series 1-5), HBM kinematic predictions in terms of displacement relative to the sled environment (excursion) were measured on the HBMs in the corresponding anatomic region as measured in the tests. For Series 1, 3 and 4 X (forwards), Y (lateral) and Z (vertical) excursions were measured at the Head, T1, T8, L2 and Pelvis. For Series 2, X and Z excursions of the Head, Shoulder, Hip, and Knee were measured. For the two far-side impacts (Series 5), X, Y and Z excursions were measured at the Head, T1, Left and Right Acromia and Pelvis.

For the lateral impact tests, Series 6, 7 and 8, HBM kinematic predictions were measured in terms of lateral velocities, integrated from accelerometer signals measured along the spine. In Series 6, lateral velocity from attached accelerometer elements was extracted from the HBM T1, T7, L3 and sacrum. For Series 7, the locations were T1, T7, T10 and the sacrum. In Series 8, the accelerometer locations were Manubrium, T1, T4, T12 and the Sacrum. In Series 6, 7, and 8, chest or abdomen deflection histories normalized by initial half width or depth, were calculated from the deflection of the HBM external torso surface, at the corresponding locations where normalized deflections were calculated from chestband results in the PMHS tests.

Table A1. Test environment models for the different test series.

Series	Description	Previously used
1	Rigid generic buck	(Piqueras-Lorente et al. 2018)
2	Rear seat sled buck with seat cushions	(Gepner et al. 2018)
3	Rigid generic buck. Generic driver airbag	(Lopez-Valdes et al. 2018)
4	Rigid generic buck, knee excursion limited	(Eggers et al. 2018)
5	Rigid generic buck with back support	(Pipkorn et al. 2018)
6	Dual sled. Sled with padded impactors (abdomen impactor offset towards subject) impacts initially stationary occupant sled	(Hwang et al. 2016)
7	Dual sled as in Series 6. Additional impactors for shoulder and upper arm. Thinner padding on impactors, adjusted for simultaneous engagement with subject	(Hwang et al. 2016)
8	Dual sled side impact buck. Production driver seat and door trim with intrusion. Side impact airbag	(Larsson et al. 2019)

Appendix B.
Result time histories from each series

Figures B1-B10 show examples of time histories of test and HBM simulation results (nominal seatbelt routing) from tests in Series 1-5. Figures B11-B19 show examples of test and HBM simulation results from Series 6-8.

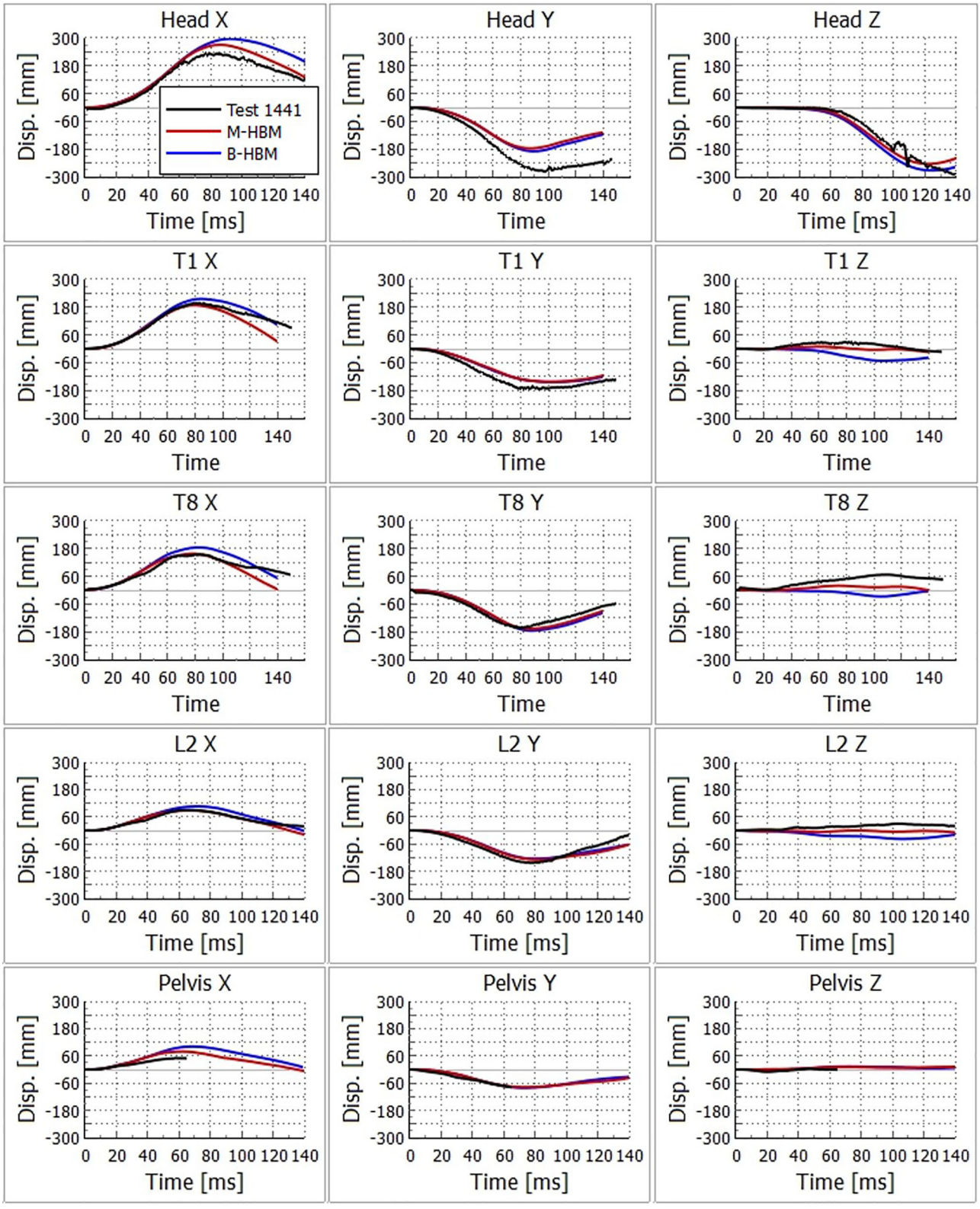

Figure B1. Series 1, Test 1441 excursion kinematics for PMHS test (black), Morphed (red) and Baseline (blue) HBMs.

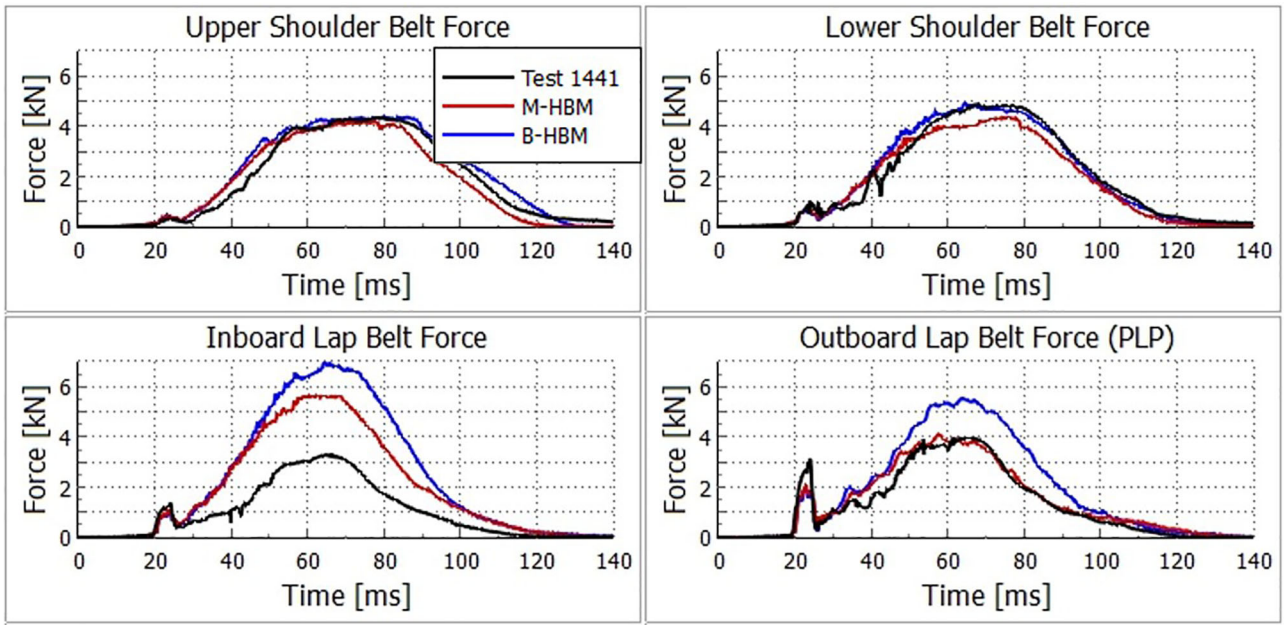

Figure B2. Series 1, Test 1441 seatbelt forces for PMHS test (black), Morphed (red) and Baseline (blue) HBMs.

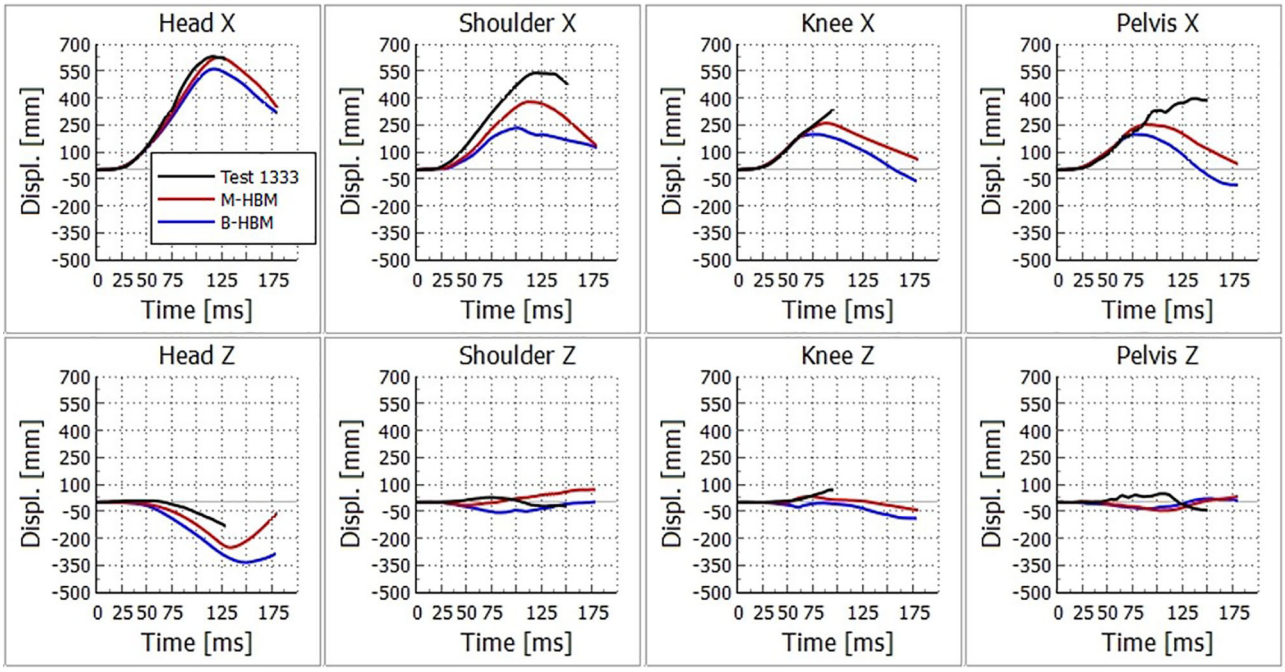

Figure B3. Series 2, Test 1333 excursion kinematics for PMHS test (black), Morphed (red) and Baseline (blue) HBMs.

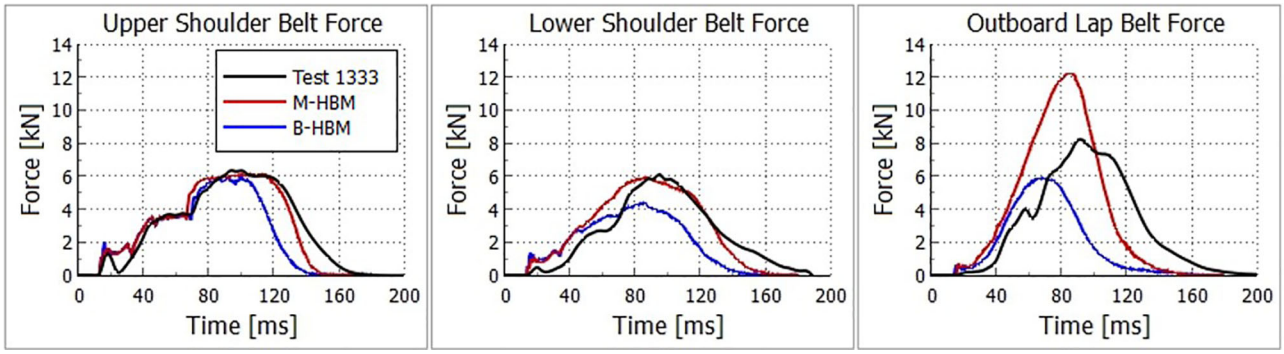

Figure B4. Series 2, Test 1333 seatbelt forces for PMHS test (black), Morphed (red) and Baseline (blue) HBMs.

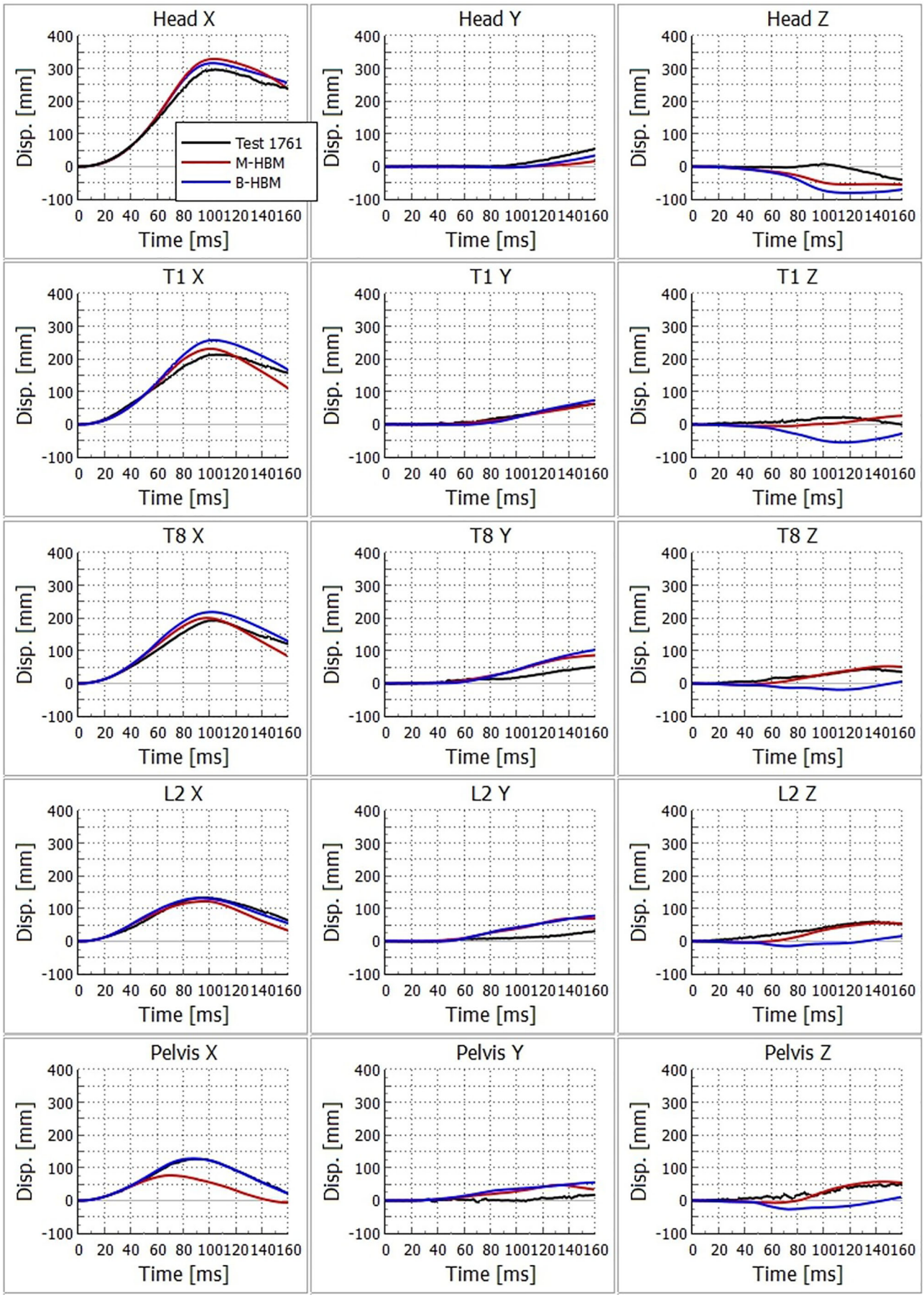

Figure B5. Series 3, Test 1761 excursion kinematics for PMHS test (black), Morphed (red) and Baseline (blue) HBMs.

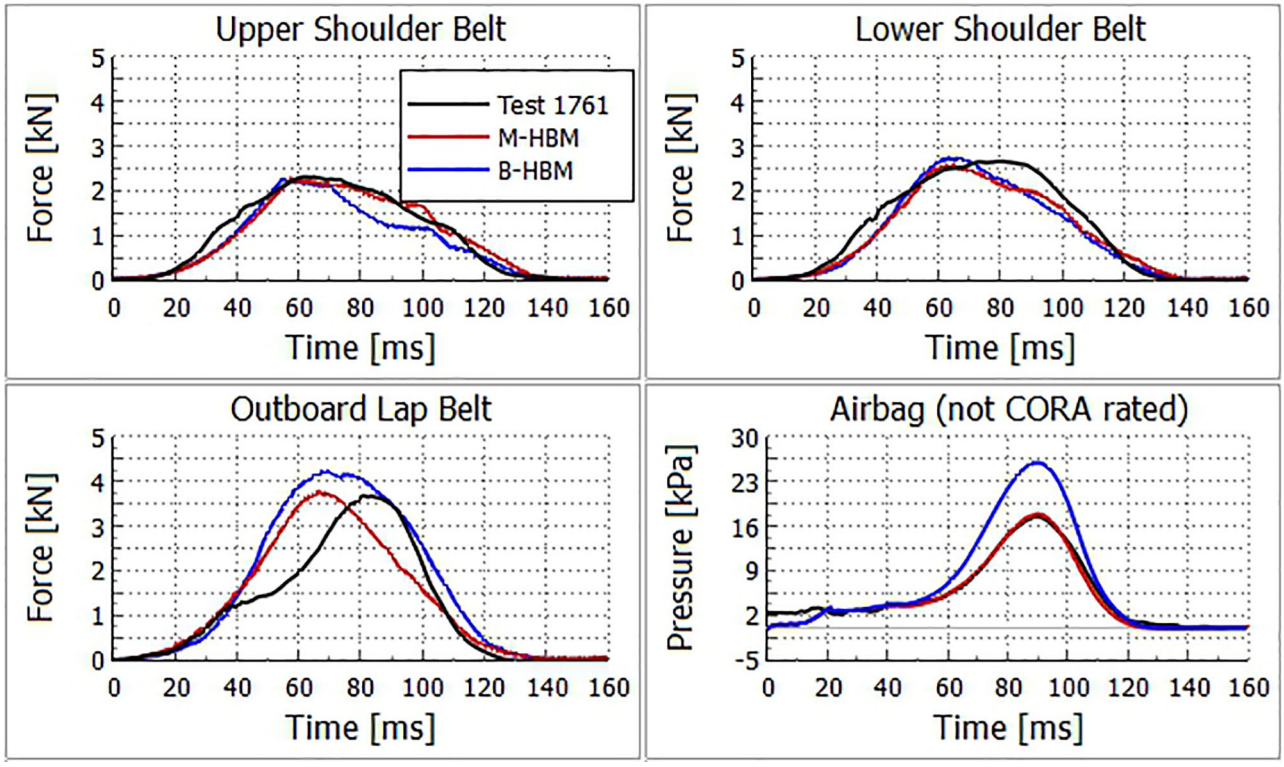

Figure B6. Series 3, Test 1761 seatbelt forces for PMHS test (black), Morphed (red) and Baseline (blue) HBMs.

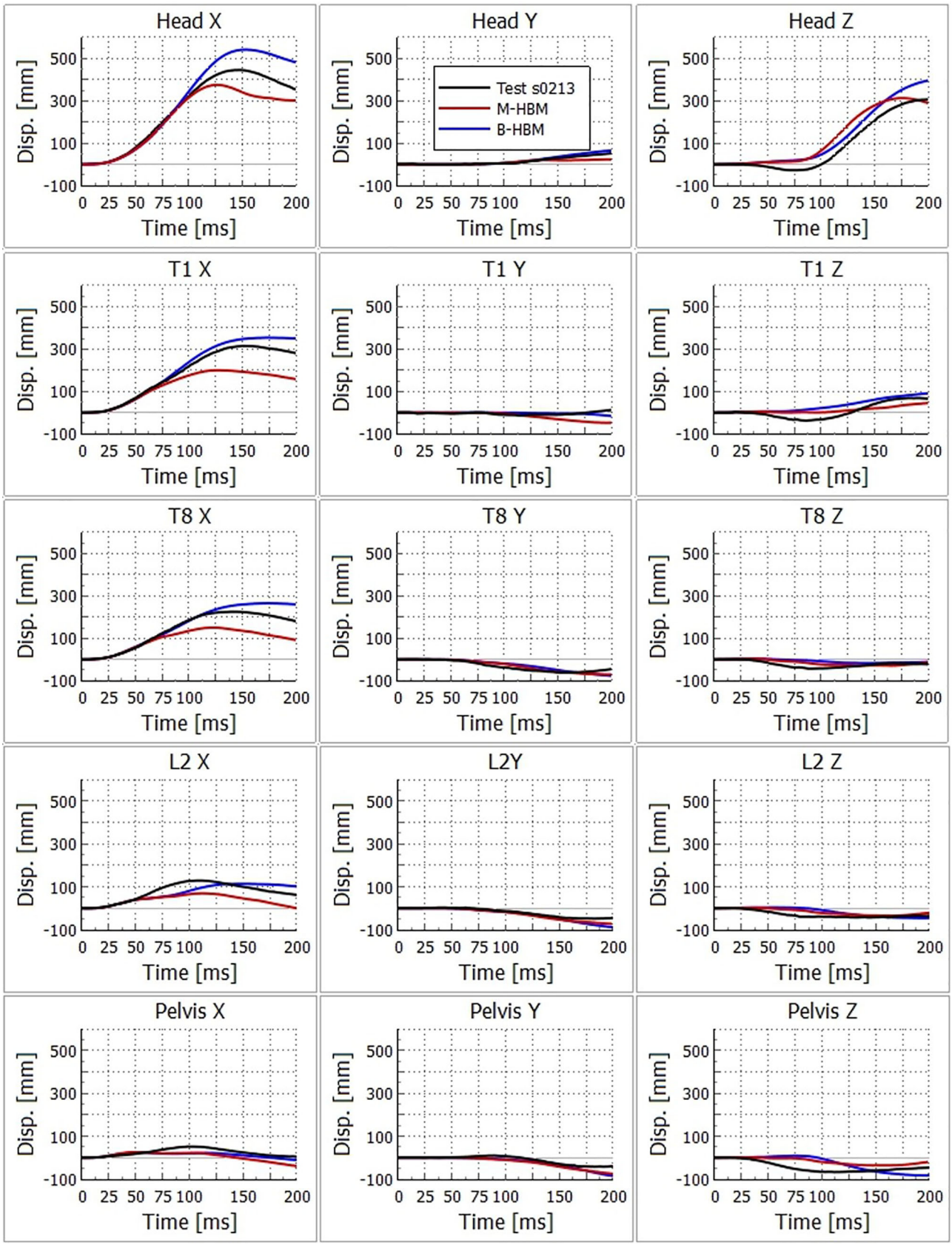

Figure B7. Series 4, Test s0213 excursion kinematics for PMHS test (black), Morphed (red) and Baseline (blue) HBMs.

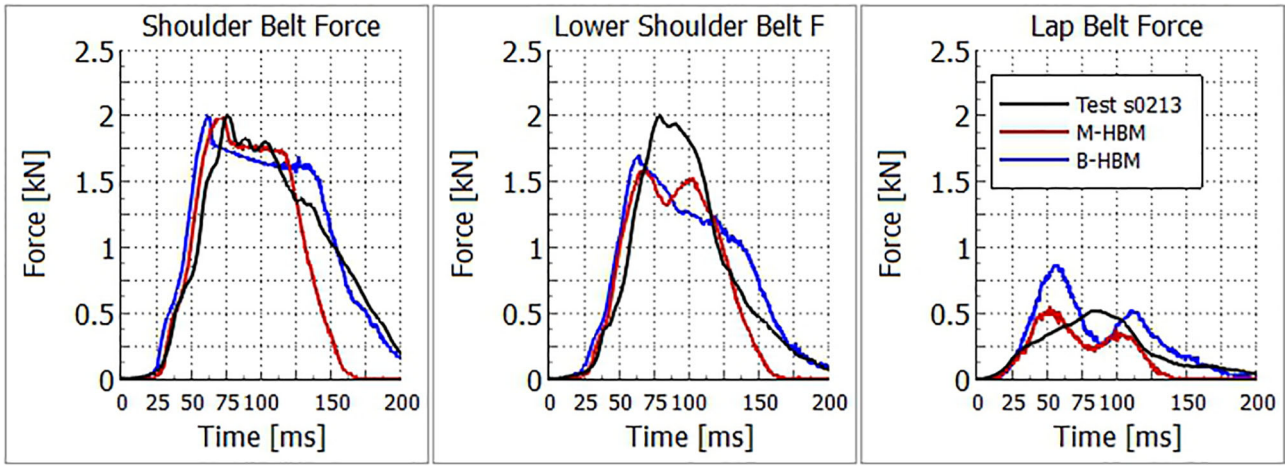

Figure B8. Series 4, Test s0213 seatbelt forces for PMHS test (black), Morphed (red) and Baseline (blue) HBMs.

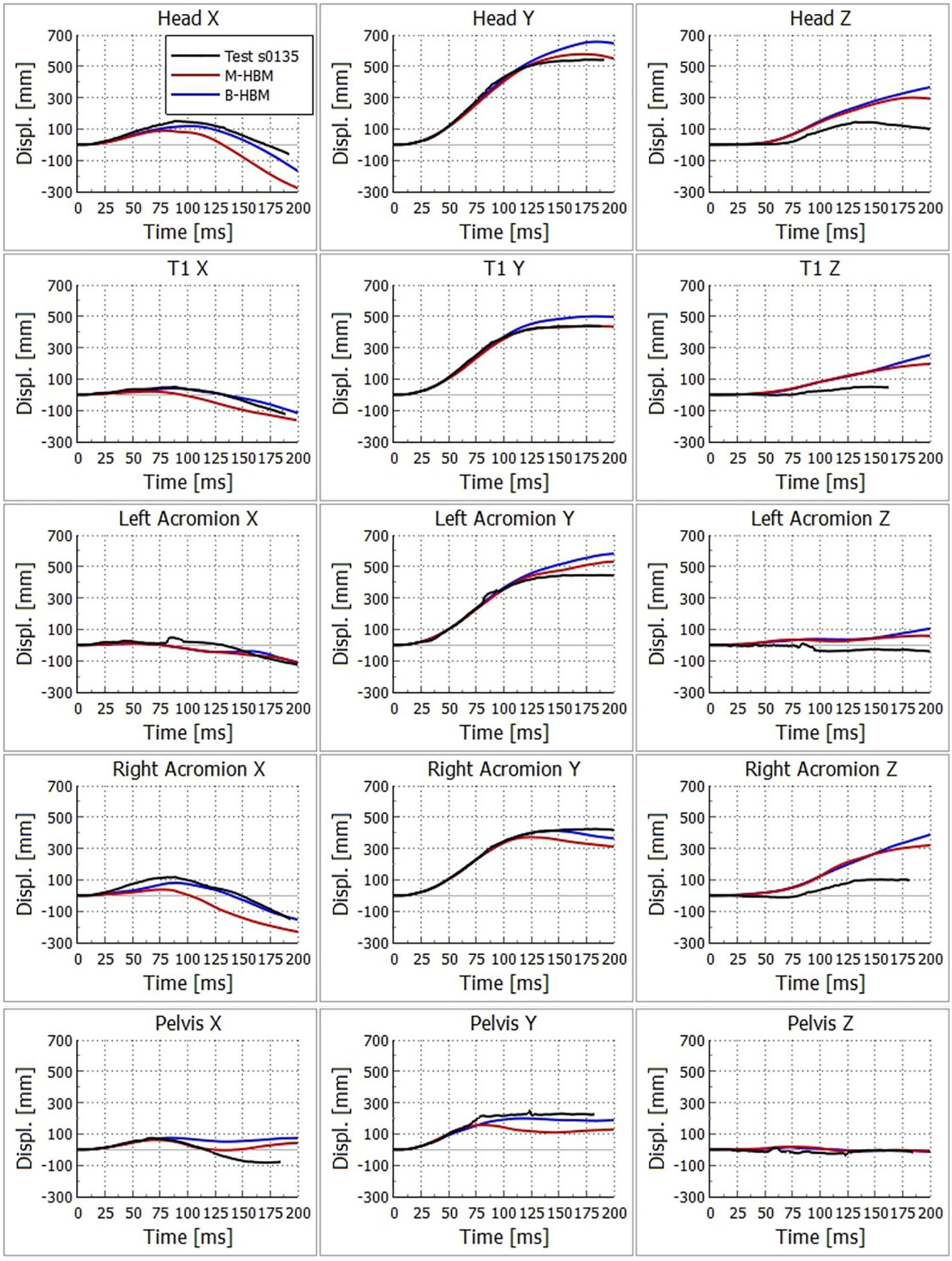

Figure B9. Series 5, Test s0135 excursion kinematics for PMHS test (black), Morphed (red) and Baseline (blue) HBMs.

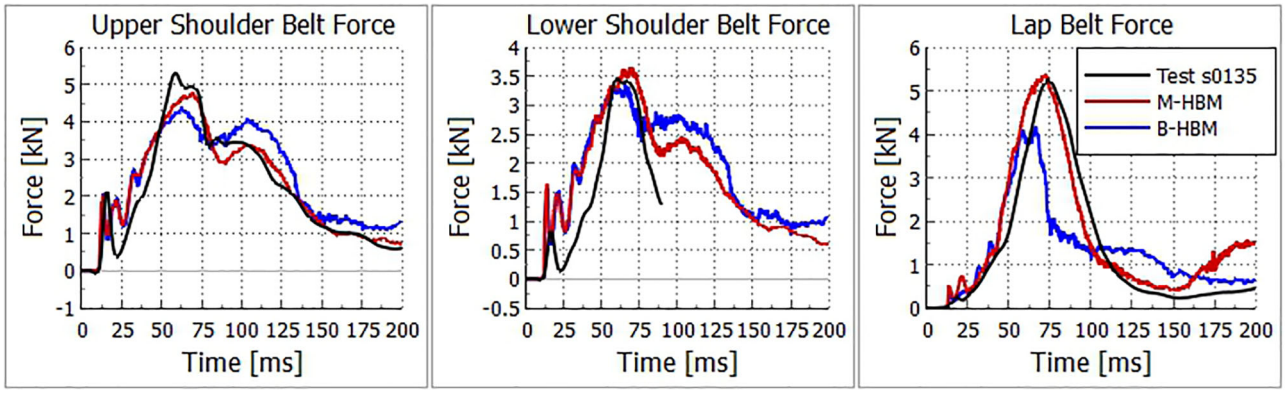

Figure B10. Series 5, Test s0135 seatbelt forces for PMHS test (black), Morphed (red) and Baseline (blue) HBMs.

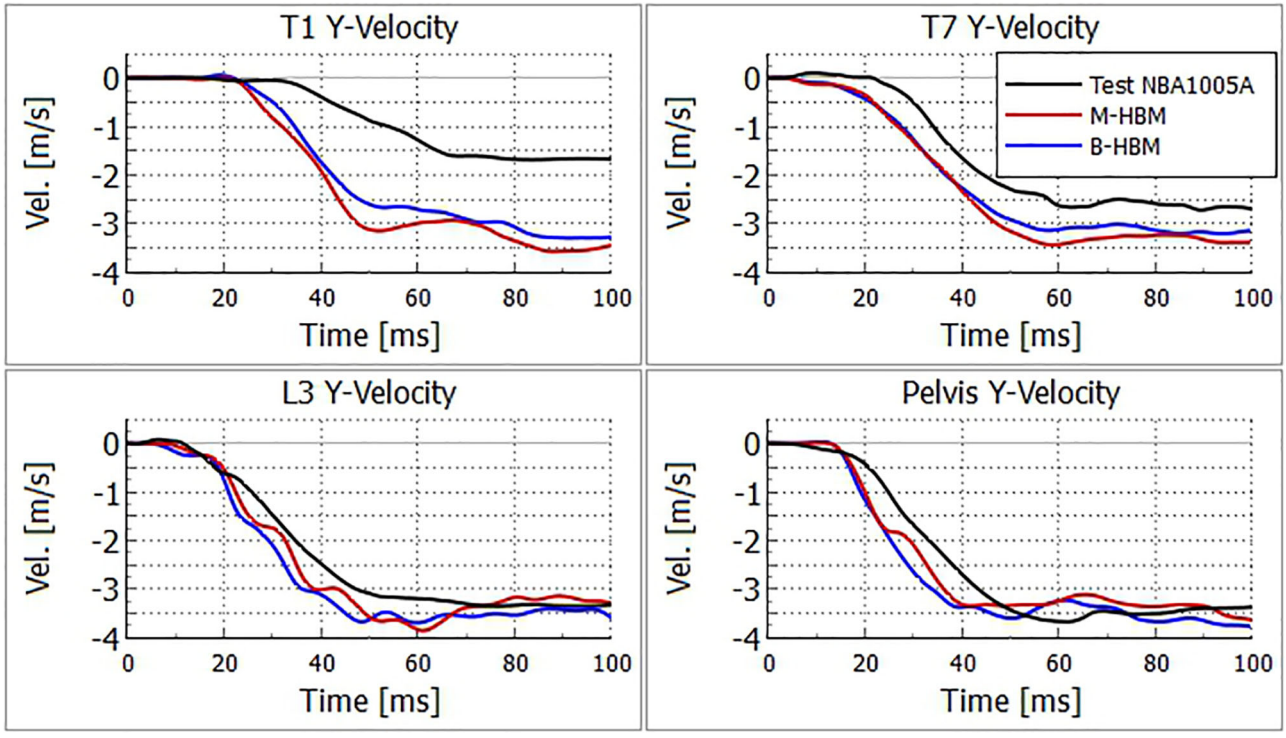

Figure B11. Series 6, Test NBA1005A lateral velocity kinematics for PMHS test (black), Morphed (red) and Baseline (blue) HBMs.

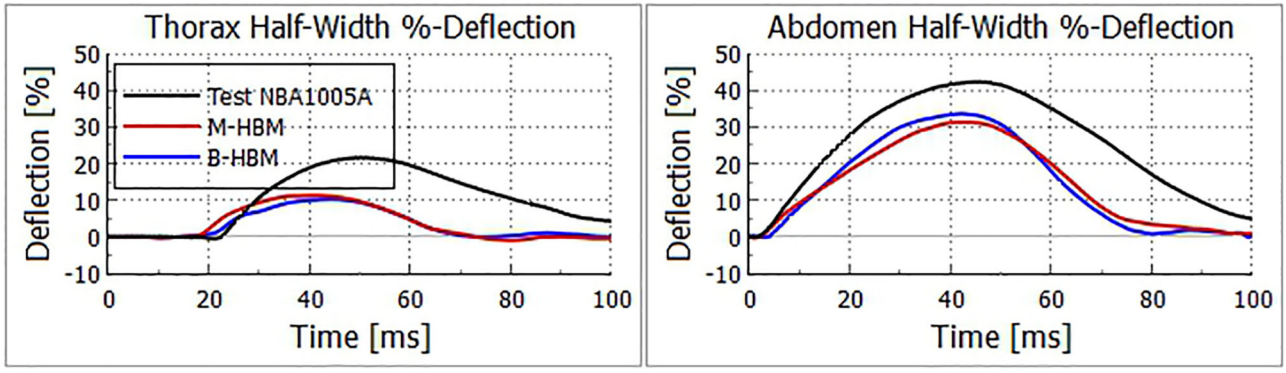

Figure B12. Series 6, Test NBA1005A chest deflections for PMHS test (black), Morphed (red) and Baseline (blue) HBMs.

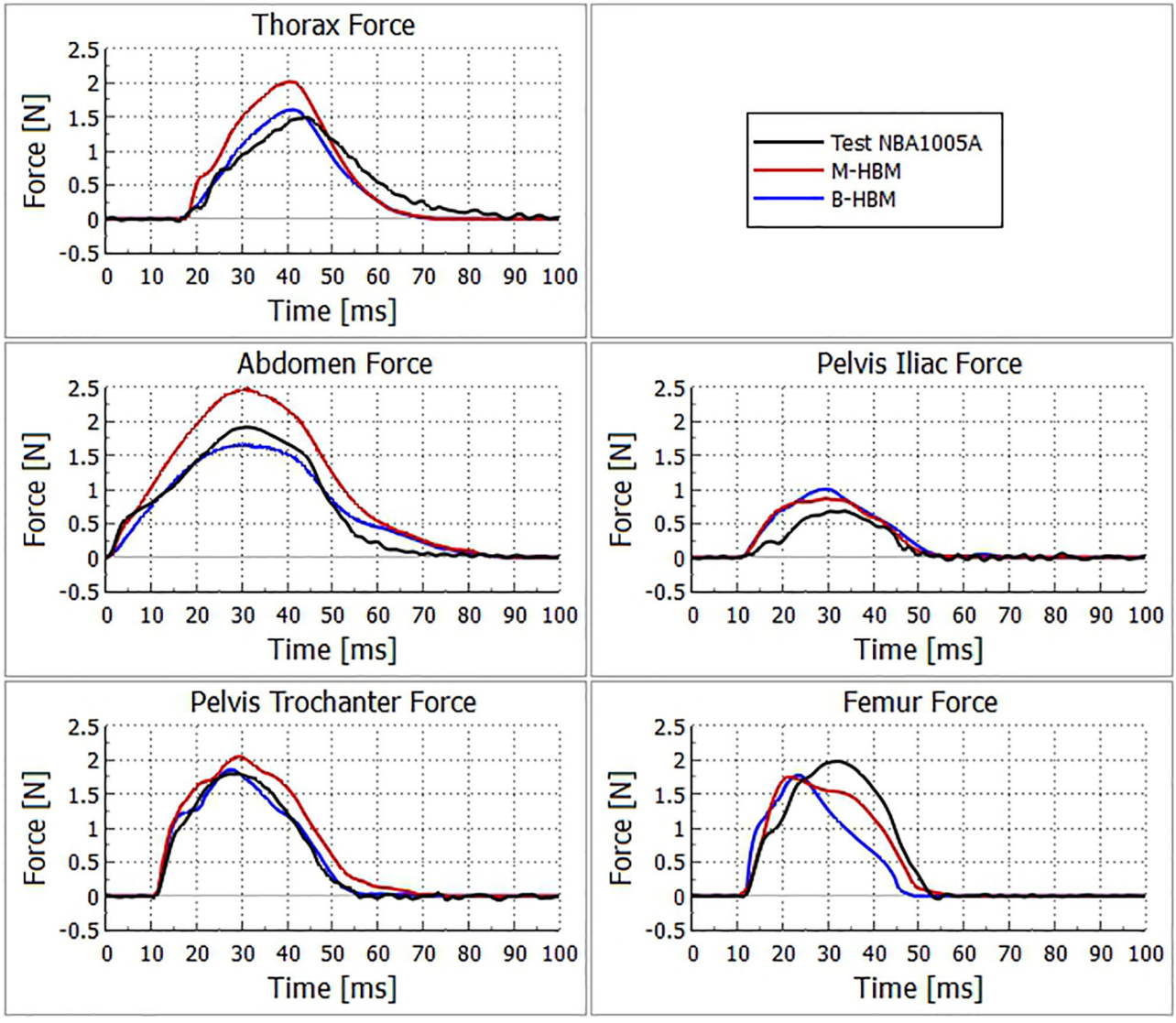

Figure B13. Series 6, Test NBA1005A impactor forces for PMHS test (black), Morphed (red) and Baseline (blue) HBMs.

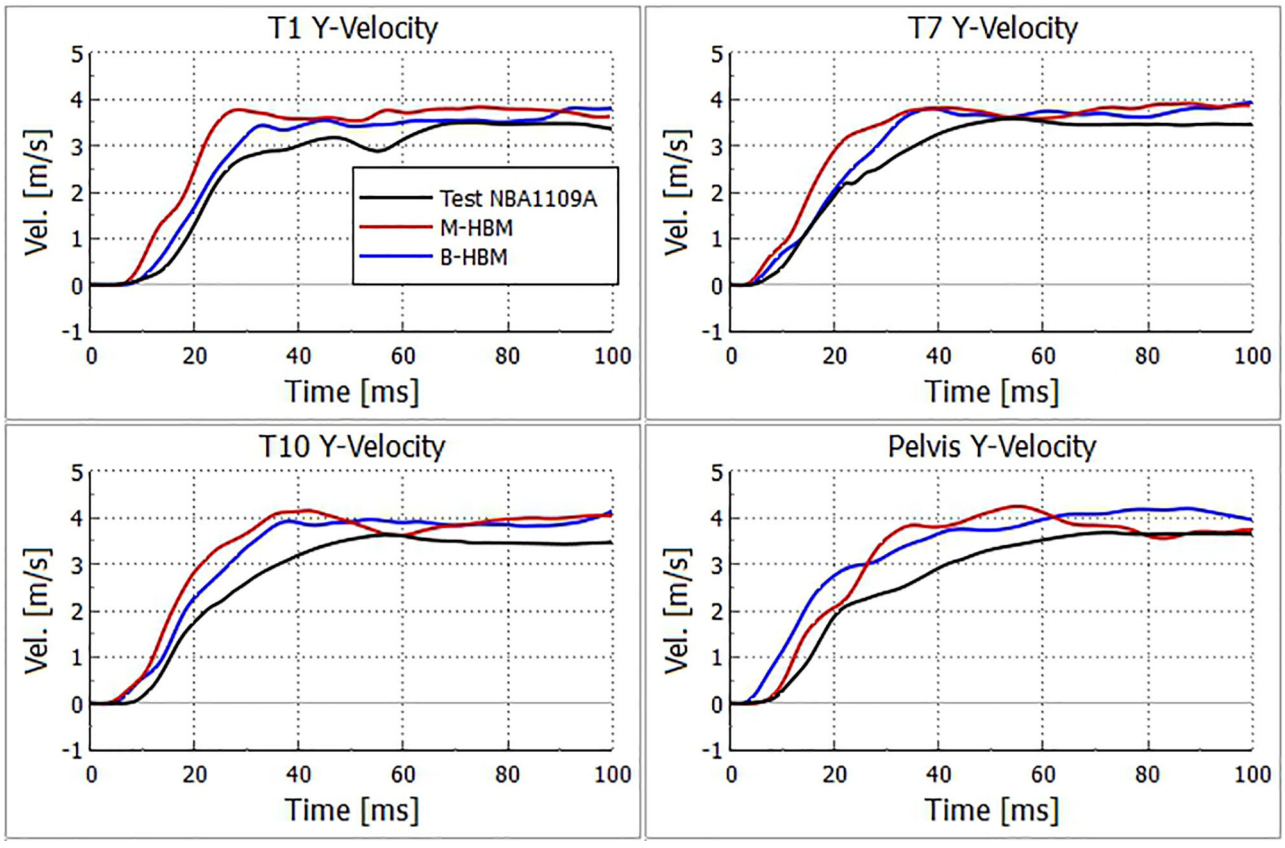

Figure B14. Series 7, Test NBA1109A lateral velocity kinematics for PMHS test (black), Morphed (red) and Baseline (blue) HBMs.

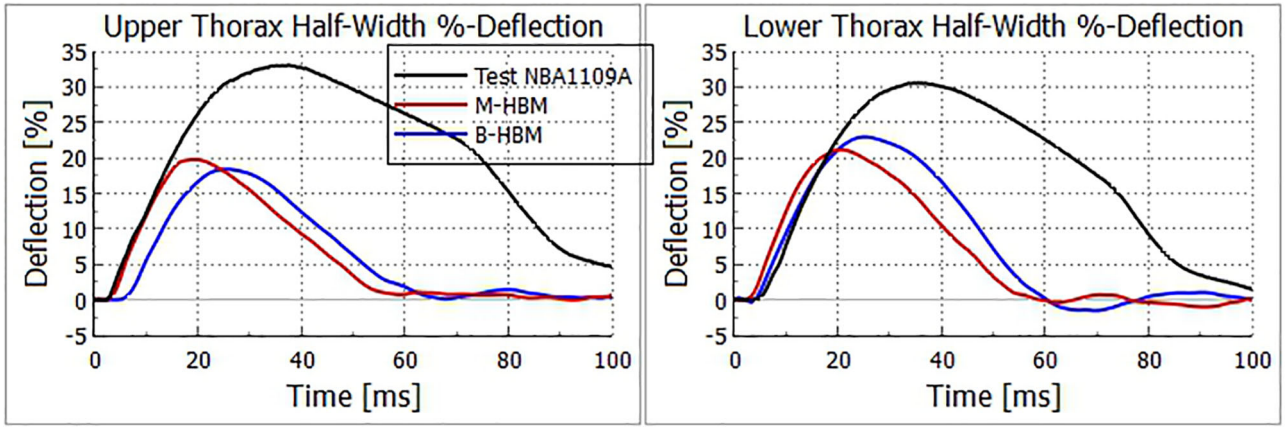

Figure B15. Series 7, Test NBA1109A chest deflections for PMHS test (black), Morphed (red) and Baseline (blue) HBMs.

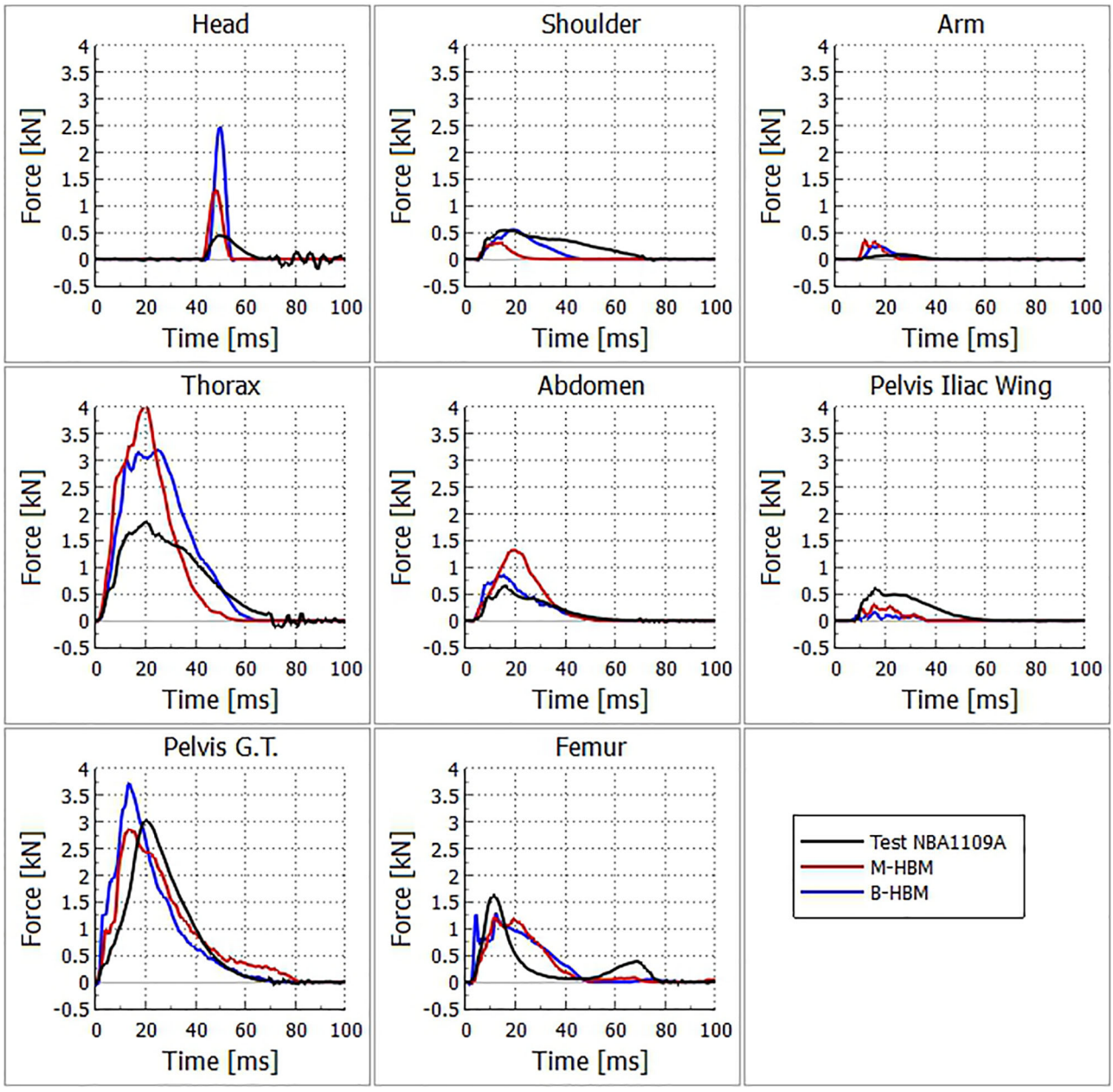

Figure B16. Series 7, Test NBA1109A impactor forces for PMHS test (black), Morphed (red) and Baseline (blue) HBMs.

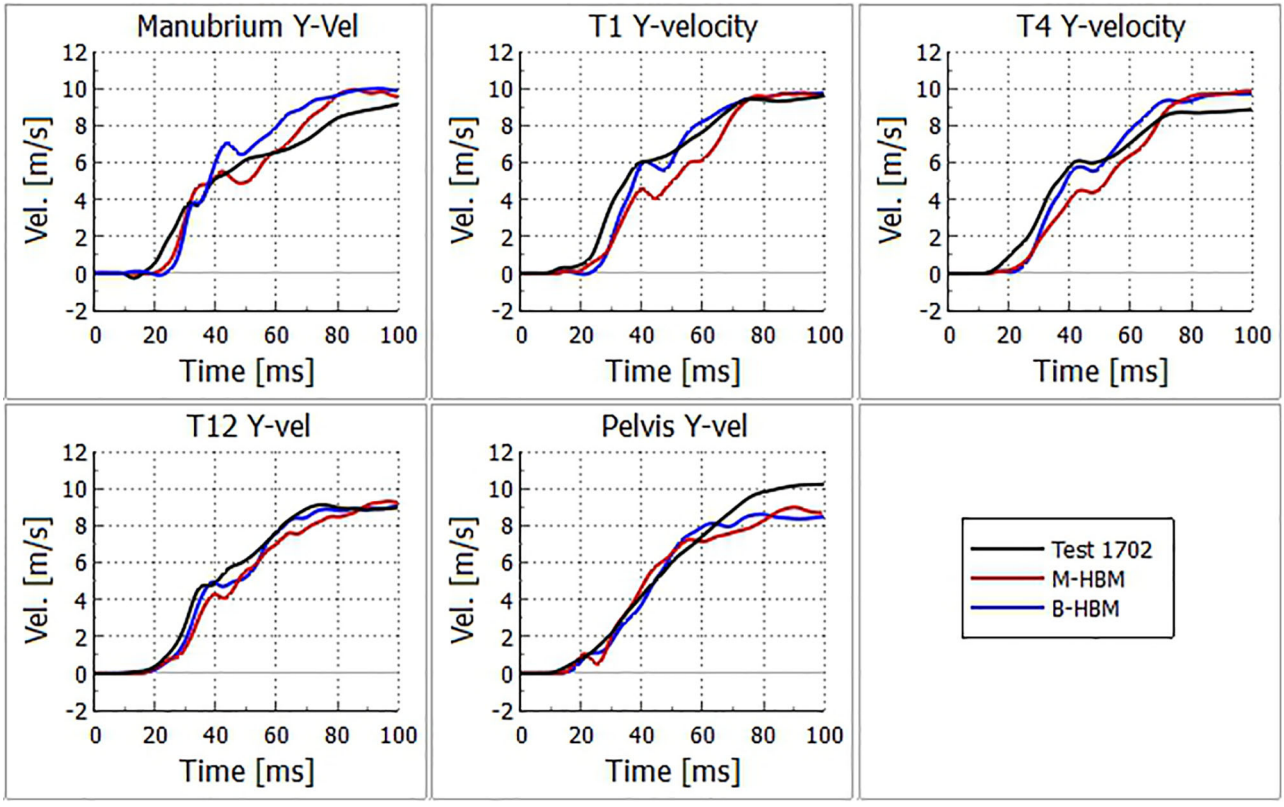

Figure B17. Series 8, Test 1702 lateral velocity kinematics for PMHS test (black), Morphed (red) and Baseline (blue) HBMs.

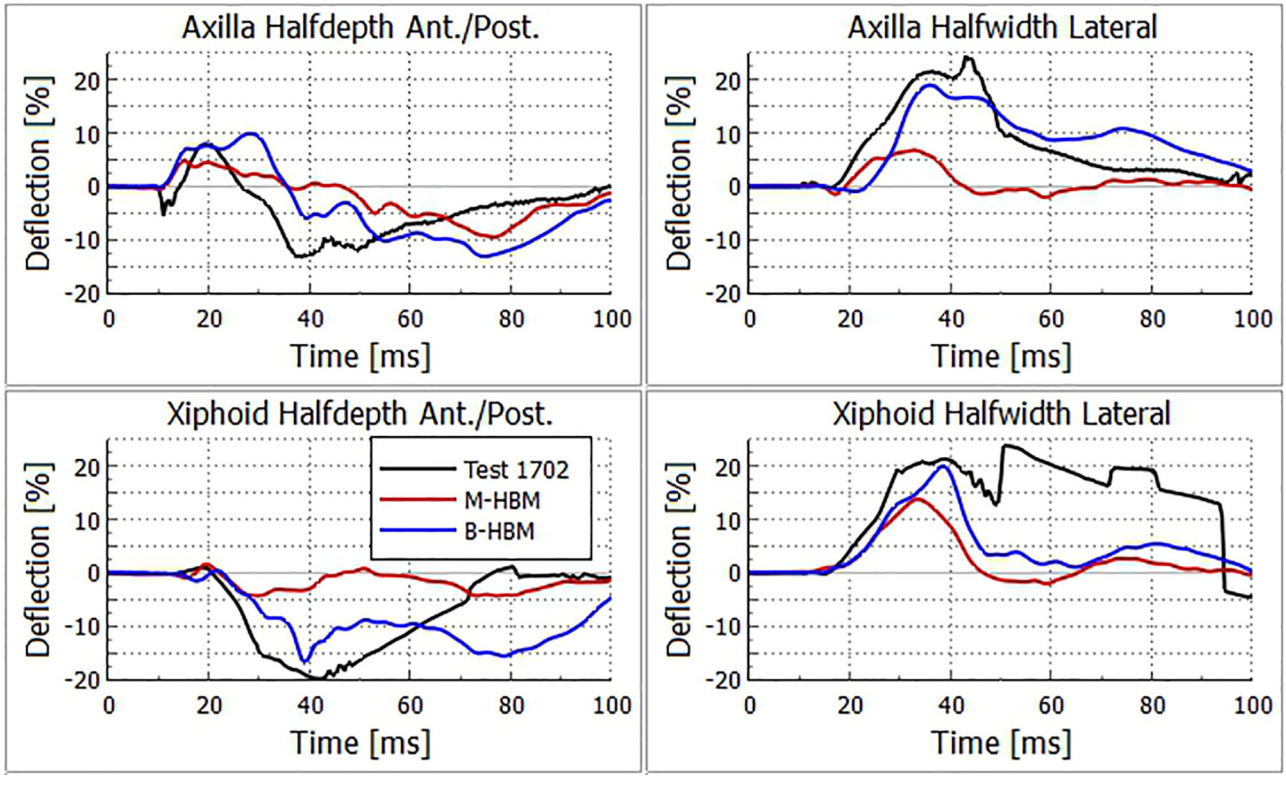

Figure B18. Series 8, Test 1702 chest deflections for PMHS test (black), Morphed (red) and Baseline (blue) HBMs.

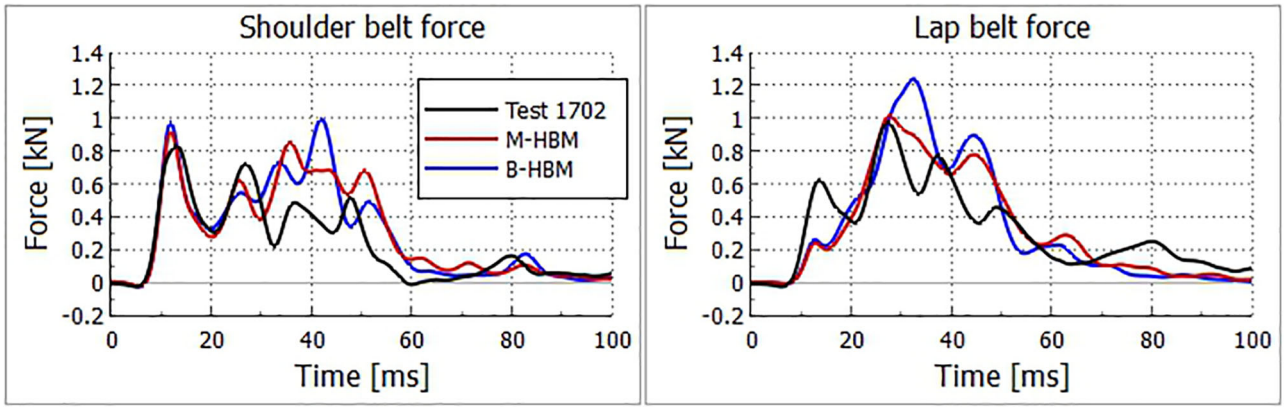

Figure B19. Series 8, Test 1702 seatbelt forces for PMHS test (black), Morphed (red) and Baseline (blue) HBMs.

Appendix C.

Kinematic snapshots

Figures C1-C5 show visual examples of test and HBM simulation kinematic results (nominal seatbelt routing) from tests in Series 1-5. Figures C6-C8 show visual examples of test and HBM simulation kinematic results from Series 6-8.

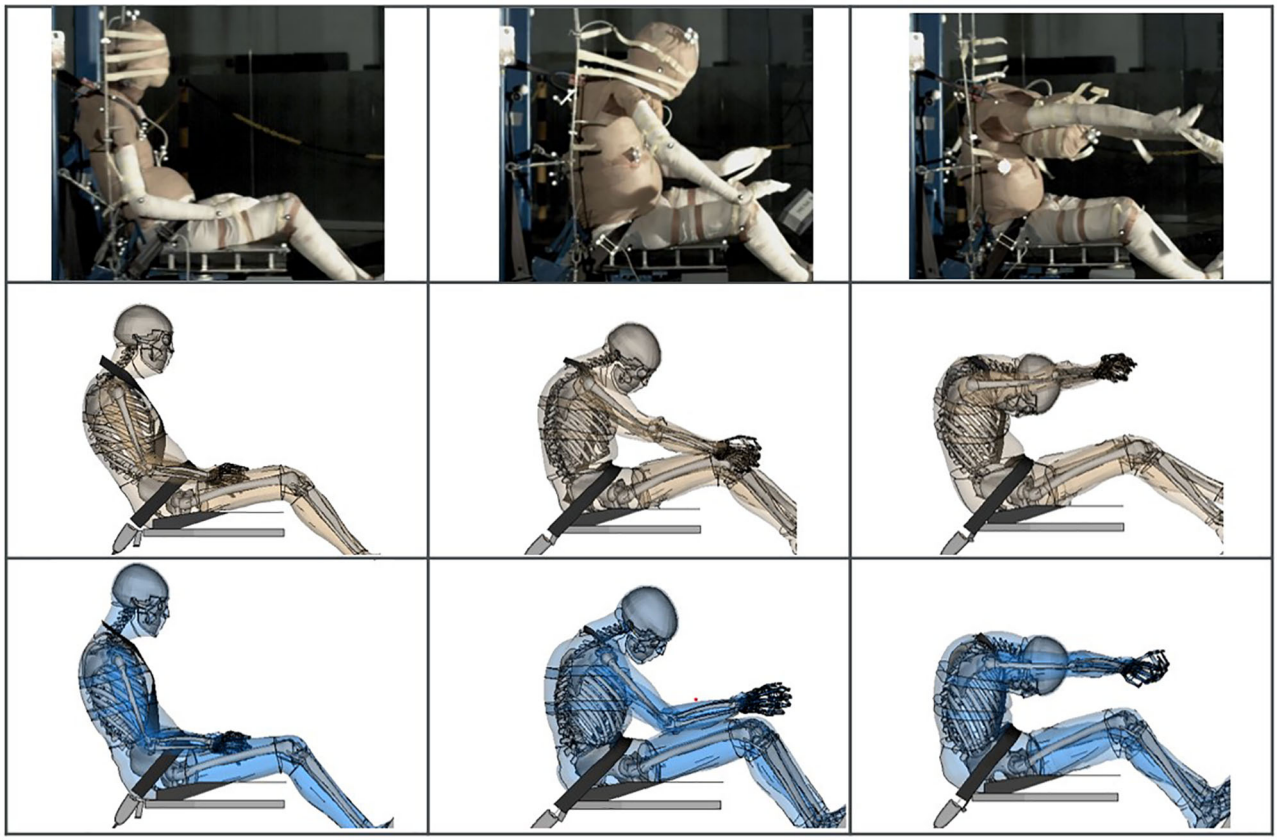

Figure C1. Kinematic frames Series 1 (oblique near-side 30°), Test 1441. Left to right: Time: 0 ms, 80 ms (test peak head forward), 120 ms. Top to bottom: PMHS test 1441, M-HBM, B-HBM.

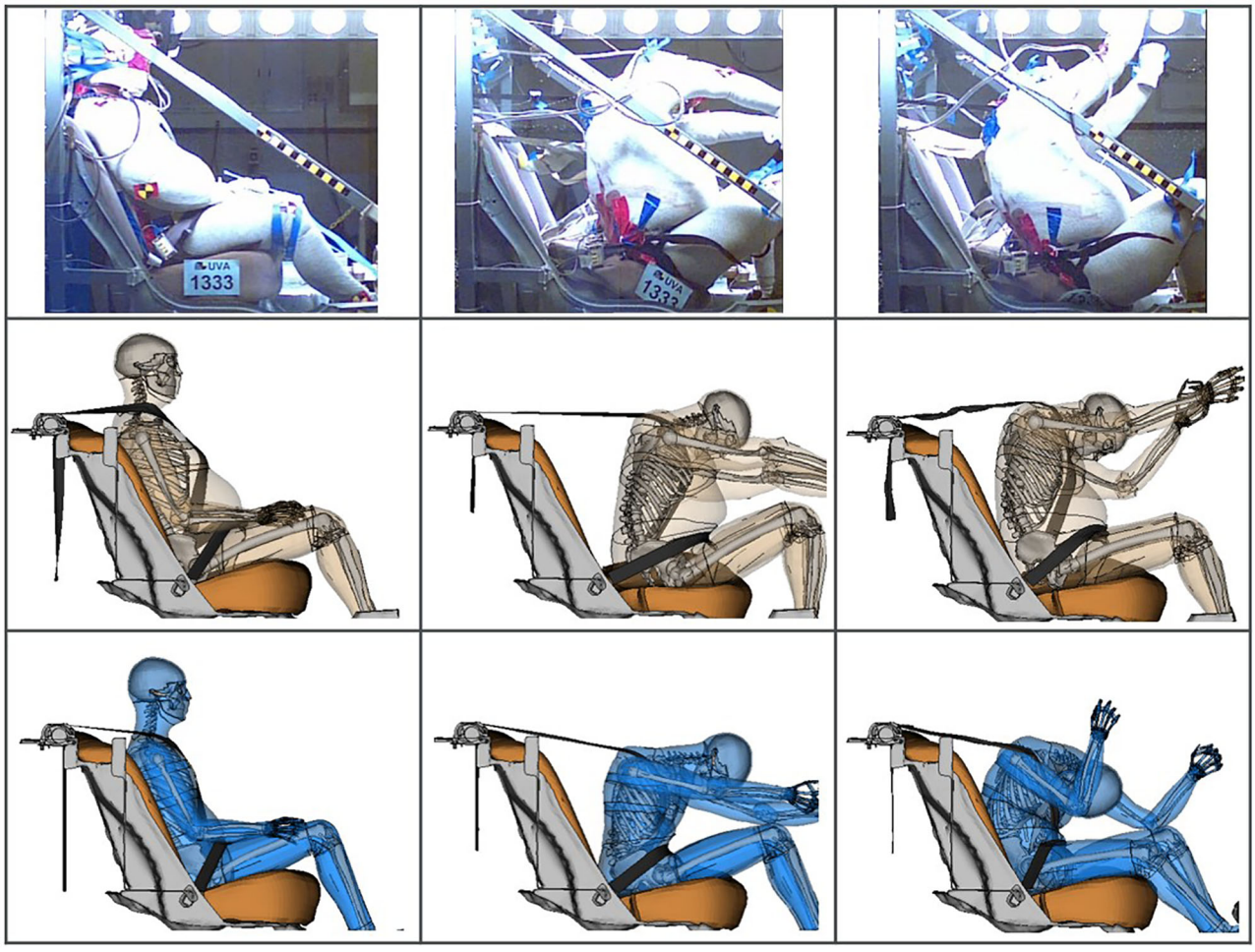

Figure C2. Kinematic frames Series 2 (frontal), test 1333. Left to right: Time: 0 ms, 112 ms (test peak head forward), 160 ms. Top to bottom: PMHS test 1333, M-HBM, B-HBM.

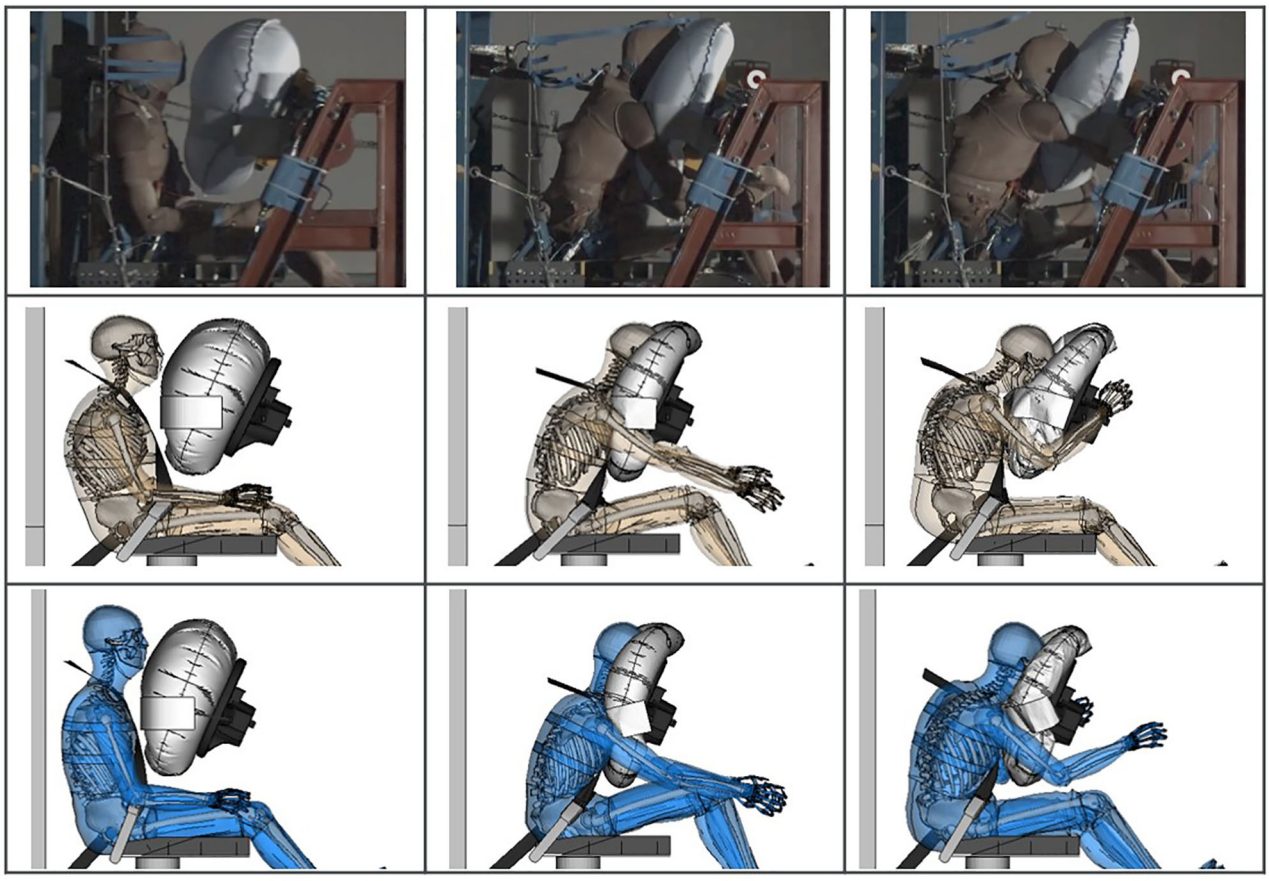

Figure C3. Kinematic frames Series 3 (frontal), test 1761 Left to right: Time: 0 ms, 100 ms (test peak head forward), 160 ms. Top to bottom: PMHS test 1761, M-HBM, B-HBM.

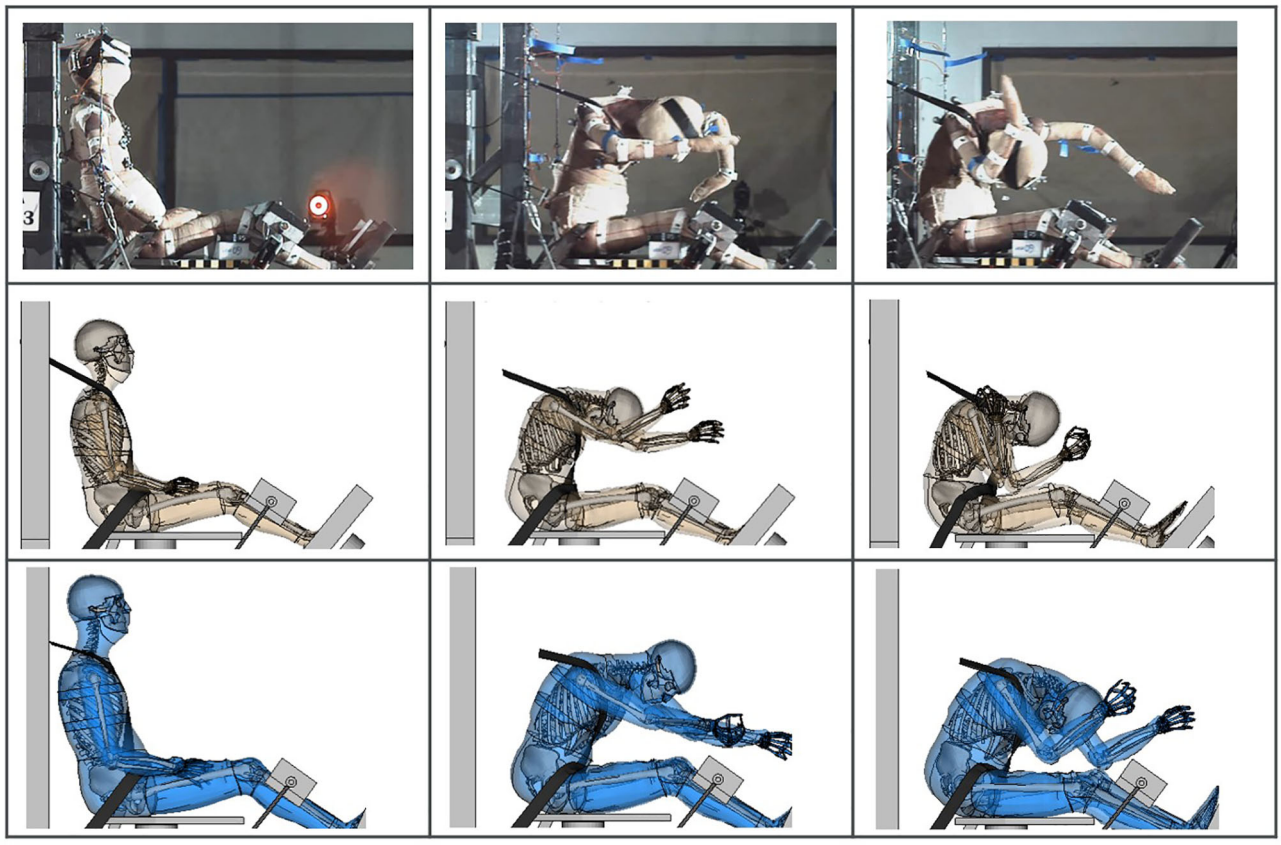

Figure C4. Kinematic frames Series 4 (frontal), test s0213 Left to right: Time: 0 ms, 148 ms (test peak head forward), 200 ms. Top to bottom: PMHS test s0213, M-HBM, B-HBM.

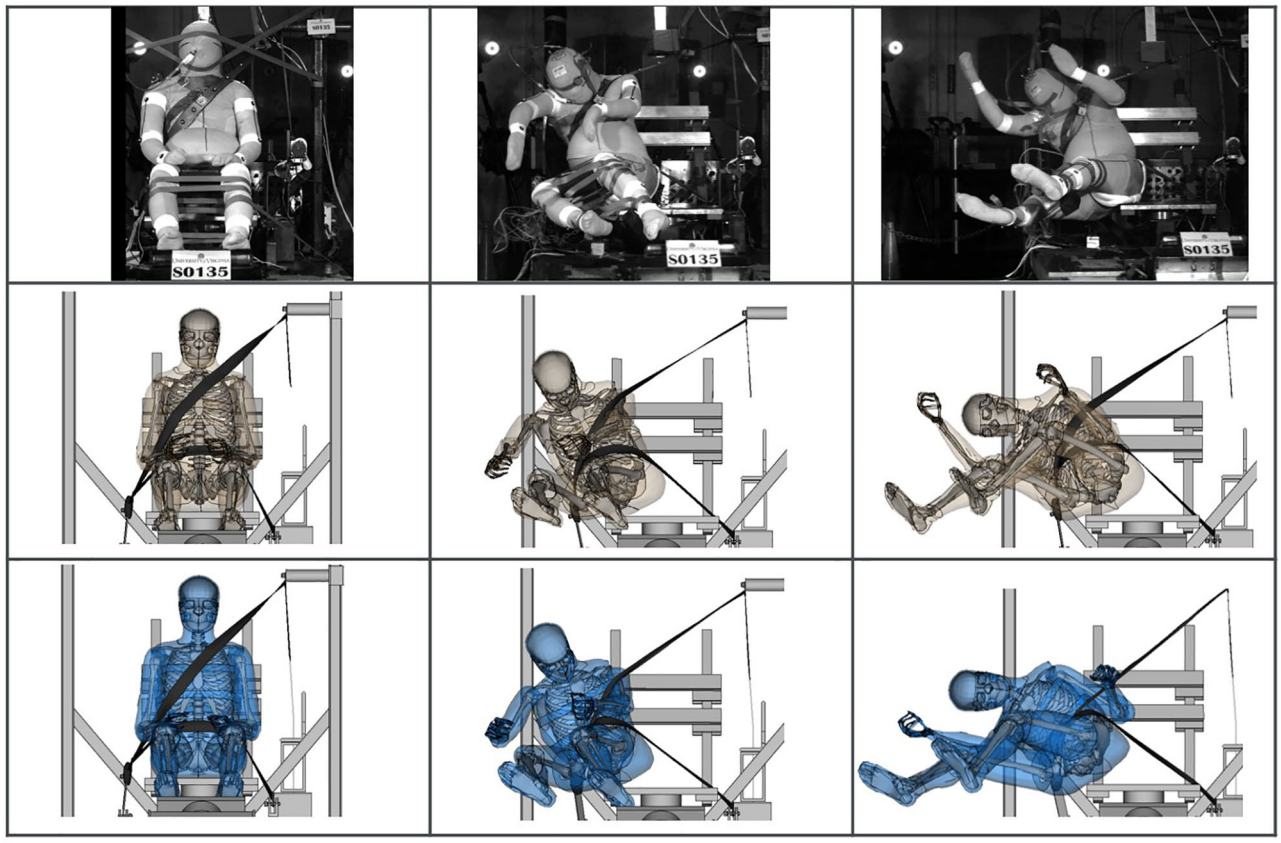

Figure C5. Kinematic frames Series 5 (oblique far-side 60°), test s0135. Left to right: Time: 0 ms, 100 ms (test peak head forward), 160 ms. Top to bottom: PMHS test s0135, M-HBM, B-HBM.

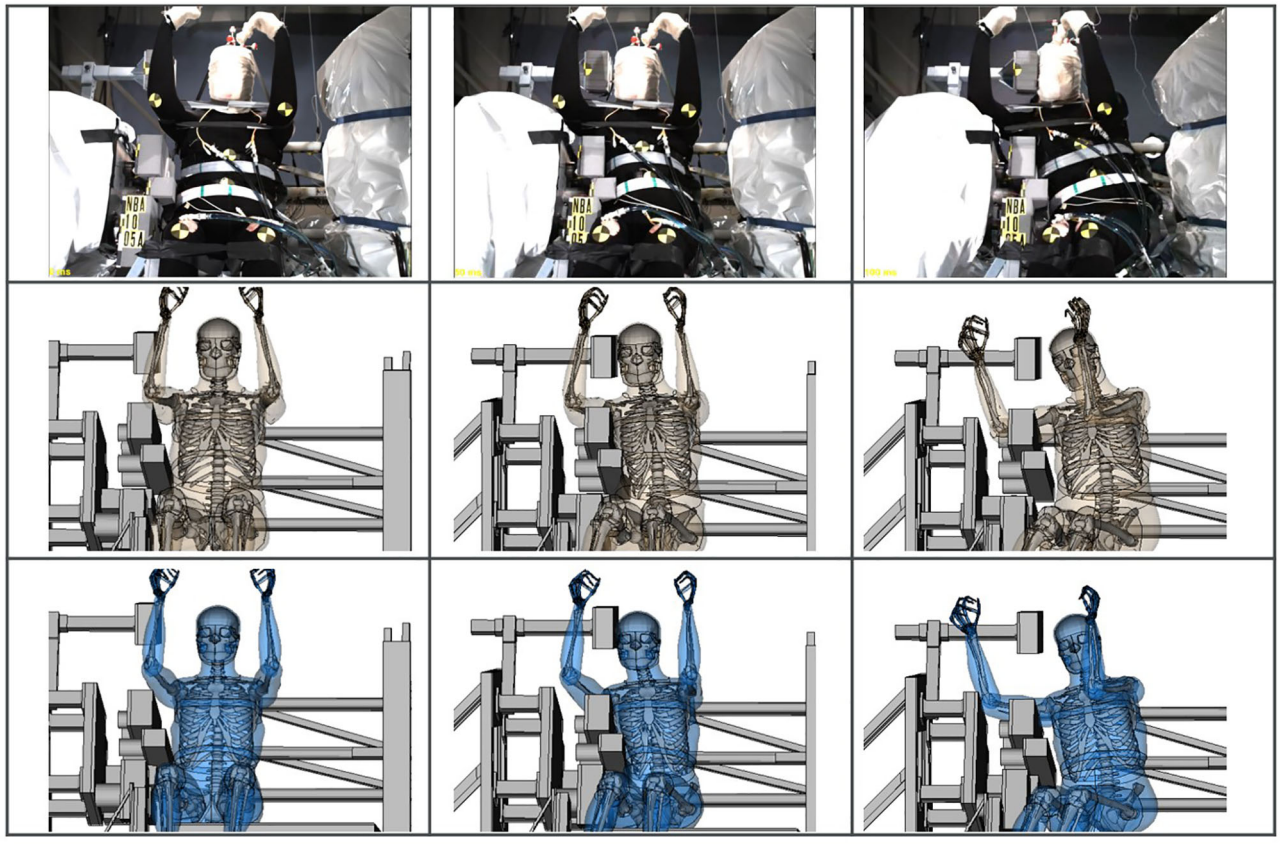

Figure C6. Kinematic frames Series 6 (lateral), test NBA1005A. Left to right: Time: 0 ms, 50 ms (test peak thorax deflection), 100 ms. Top to bottom: PMHS test NBA1005A, M-HBM, B-HBM.

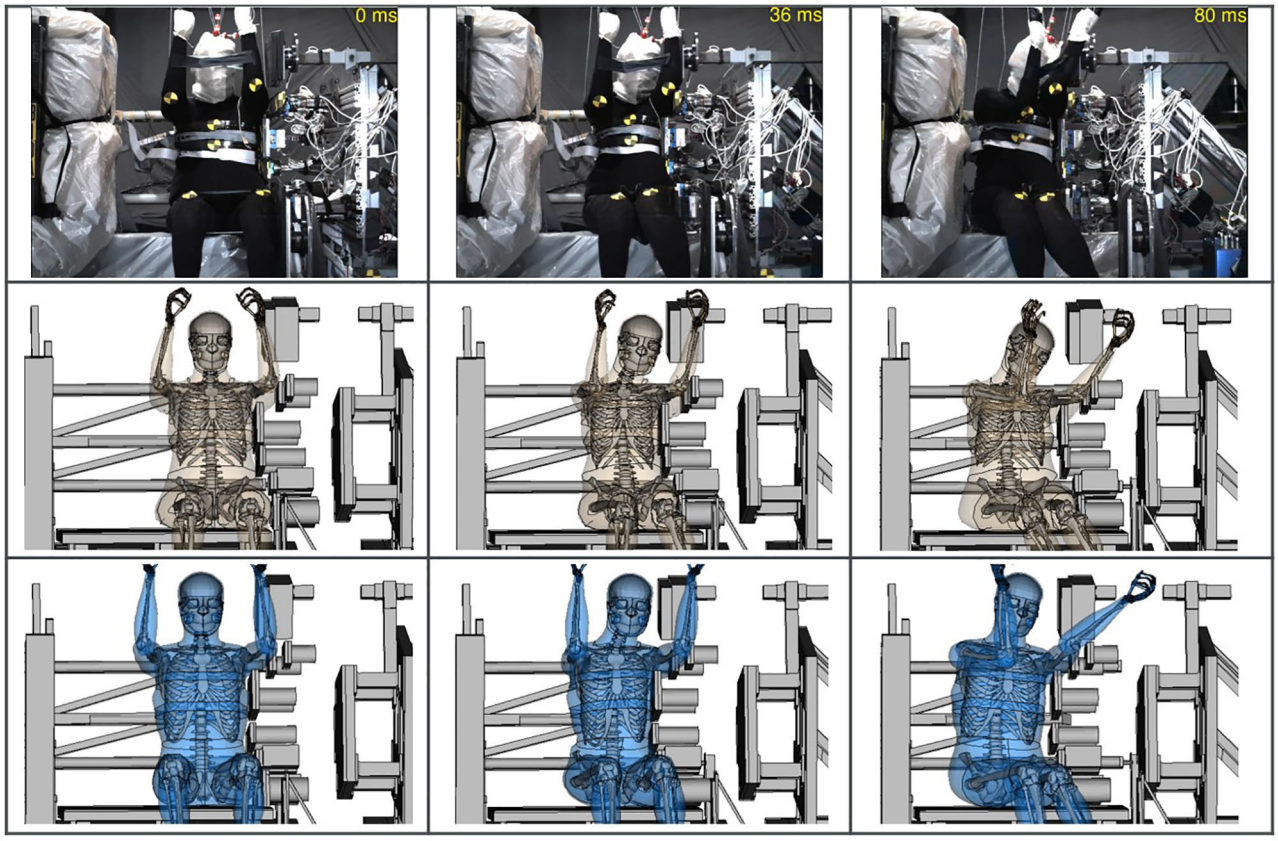

Figure C7. Kinematic frames Series 7 (lateral), Test NBA1109A. Left to right: Time: 0 ms, 36 ms (test peak thorax deflection), 80 ms. Top to bottom: PMHS test NBA1109A, M-HBM, B-HBM.

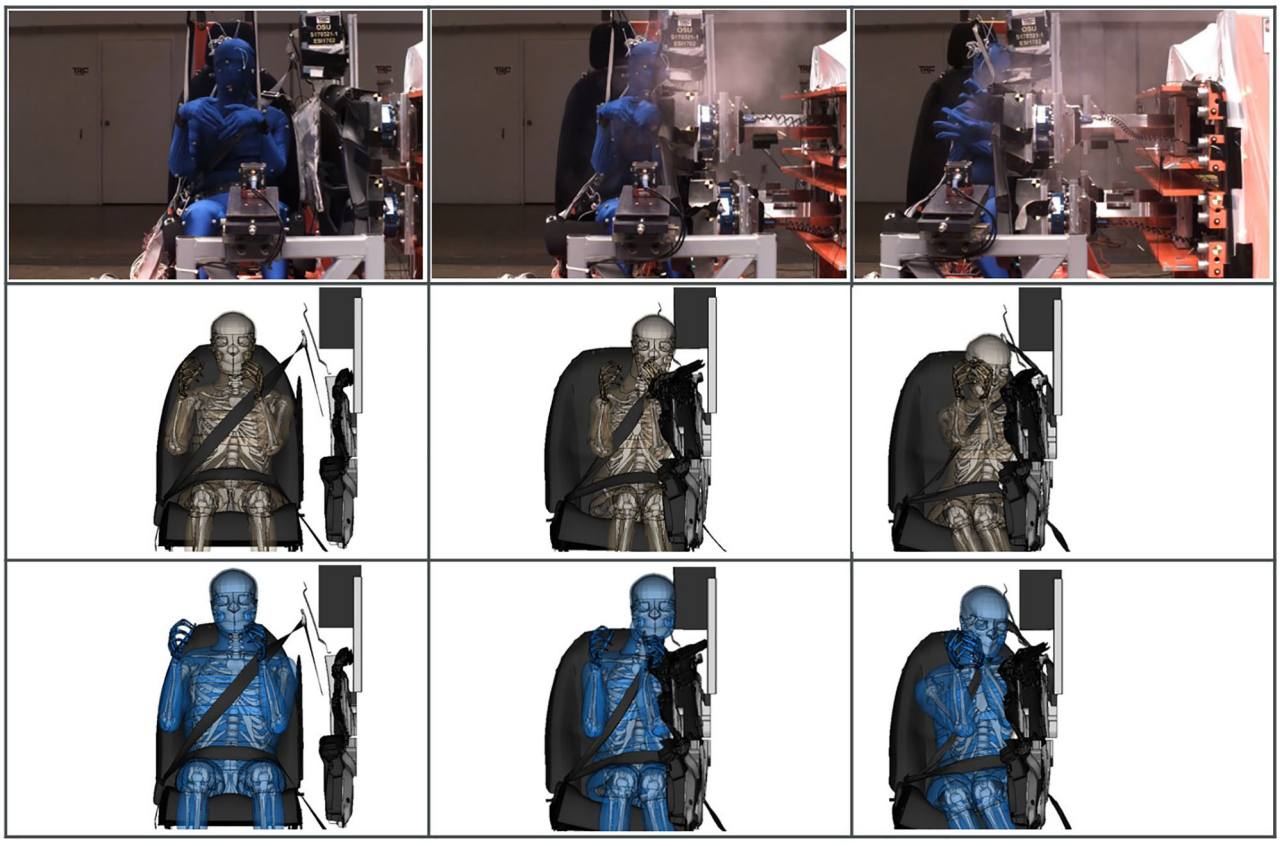

Figure C8. Kinematic frames Series 8 (lateral), Test 1702. Left to right: Time: 0 ms, 41 ms (test peak thorax lateral deflection), 80 ms. Top to bottom: PMHS test 1702, M-HBM, B-HBM.